A procedure for stable electrical measurements on a rock sample against high contact resistance as a prerequisite for electrical tomography

Takeshi Suzuki (suzuki.takeshi.38n@st.kyoto-u.ac.jp)
Graduate School of Science, Kyoto University https://orcid.org/0000-0001-7886-7729
Ryokei Yoshimura
Disaster Prevention Research Institute, Kyoto University
Ken'ichi Yamazaki
Miyazaki Observatory, Research Center for Earthquake Prediction, Disaster Prevention Research Institute, Kyoto University
Naoto Oshiman
Disaster Prevention Research Institute, Kyoto University

Technical report

Keywords: Multi-point measurement, small electrode, current injection, voltage measurement, resistivity measurement, contact resistance, absolute humidity, differential method, granite, measurement environment

Posted Date: February 17th, 2021

DOI: https://doi.org/10.21203/rs.3.rs-49036/v2

Version of Record: A version of this preprint was published at Earth, Planets and Space on June 7th, 2021. See the published version at https://doi.org/10.1186/s40623-021-01446-9.

Title: A procedure for stable electrical measurements on a rock sample against high contact resistance as a prerequisite for electrical tomography

Author #1(Corresponding author): Takeshi Suzuki, Graduate School of Science, Kyoto University, Gokasho, Uji, Kyoto 611-0011, Japan, suzuki.takeshi.38n@st.kyoto-u.ac.jp

Author #2: Ryokei Yoshimura, Disaster Prevention Research Institute, Kyoto University, Gokasho, Uji, Kyoto 611-0011, Japan, ryokei@eqh.dpri.kyoto-u.ac.jp

Author #3: Ken'ichi Yamazaki, Miyazaki Observatory, Research Center for Earthquake Prediction, Disaster Prevention Research Institute, Kyoto University, 3884, Kaeda, Miyazaki 889-2161, Japan, kenichi@rcep.dpri.kyoto-u.ac.jp

Author #4: Naoto Oshiman, Disaster Prevention Research Institute, Kyoto University, Gokasho, Uji, Kyoto 611-0011, Japan, osman@eqh.dpri.kyoto-u.ac.jp

Abstract

As a basis for the electrical tomography of laboratory-scale rock samples (~ 10 cm), we developed a procedure for stable, multi-point, electrical measurement

on rock samples that is effective even at high contact and sample resistance. Electrodes were strongly attached to the surface of high-resistivity rock using conductive and adhesive epoxy. Sustained current injection for long periods into high-resistance rocks was fulfilled using a constant direct current source with high internal resistance. Accurate voltage measurement across the high-resistance rock was accomplished by differential measurement using two high input resistance voltmeters. Measurements of high resistance also require a stable measurement environment: the temperature and humidity in the laboratory were controlled using an air conditioner, a humidifier, a dehumidifier, and a vinyl tent. Signal noise arising from human activities was eliminated by the remote operation of the measuring equipment and switching terminal. The proposed measurement procedure was evaluated in terms of the stability and accuracy of measured values and its applicability to electrical tomography. To assess measurement stability, we performed multiple measurements of a dry granite sample at various levels of absolute humidity. Our procedure recorded highly reproducible measurements under each humidity condition. The observed changes in measured values with absolute

humidity indicate the importance of stabilising the temperature and humidity conditions in the laboratory. Applying our technique to multiple plastic samples with known resistivity confirmed its accuracy. To evaluate its applicability to electrical tomography, we measured the potential distribution on a dry granite surface in response to an injected current using a simple 40-electrode array. The potential distribution measured by our procedure agreed well with that predicted by forward modelling, demonstrating the robustness of our procedure in array measurements, and thus indicating its potential applicability to tomographic measurements for a variety of targets even under severe conditions including the relative dryness of ambient humidity.

Keywords

Multi-point measurement, small electrode, current injection, voltage measurement, resistivity measurement, contact resistance, absolute humidity, differential method, granite, measurement environment

Main Text

1. Introduction

Electrical resistivity estimated through geo-electromagnetic observations is crucial to understanding underground strata and their compositions. Its spatial variation qualitatively reflects the tectonic and geological setting. However, quantitative interpretation of the obtained resistivity and its spatial variation is not easy because subsurface resistivity is complexly affected by many factors. Its proper interpretation requires a good understanding of the rocks' electrical properties. Therefore, electrical measurements of a variety of rock samples across a wide range of conditions and spatial scales are essential.

Previous studies have measured the resistivities of various rock samples in a variety of conditions. For example, Brace et al. (1965) measured the resistivity of granite saturated with salt and tap water at high pressure. Coster (1948) measured the resistivity of granite, gabbro, basalt, peridotite, gneiss, and eclogite at various temperatures up to 1,000 °C. Fuji-ta et al. (2004) studied the electrical resistivity of granulite at 1.0 GPa and 300–890 K, and Fuji-ta et al. (2007) investigated the electrical resistivity of gneiss

at 1.0 GPa and up to 1000 K. These previous studies focused only on the bulk resistivity of rock samples. Kariya and Shankland (1983) systematically discussed the properties of bulk resistivity by compiling experimental results. In contrast, few experiments have measured the internal resistivity structure of rocks, despite its potentially usefulness in providing important information for the interpretation of electromagnetic survey results. At present, anomalies or contrasts detected by electromagnetic surveys in their resolvable scale (i.e., on the order of km) are frequently attributed to structures with small scales such as fault planes and rupture zones. However, little research has considered the ways that small-scale structures in electrical resistivity appear in larger-scale images of electrical resistivity or how the resistivities of constituents appear in bulk resistivity values. If we can determine the internal structures of rock samples at the laboratory scale together with their bulk resistivities, we may be able to establish quantitative descriptions of electrical resistivities at different spatial scales. Therefore, not only measuring the bulk resistivity of a small sample but also imaging its internal structure, is desirable for interpreting large-scale electrical resistivity structures.

In order to investigate the internal resistivity structure of a rock sample, the potential

distribution on its surface must be measured with a sufficient spatial resolution by using multiple small electrodes attached to it. In addition, large samples are inevitable when measuring artificially fractured rocks, because the precisely controlled compression required to make fractures cannot be applied to small samples. Therefore, measurements must use small electrodes and the sample must be large in order to allow a measurement array to be applied without the electrodes overlapping. The small size of the electrodes and the large size of the sample inevitably increase the contact resistance and sample resistance, respectively, hampering stable current injection and voltage measurement. Therefore, electrical tomography is generally difficult. Some previous studies of electrical tomography (e.g., Borsic et al. 2005, Stacey 2006) measured only high porosity samples under high water saturation, and thus avoided the major difficulties of high contact and sample resistance. Stacey (2006) reported that electrical tomography can only be performed with sufficient water saturation to provide proper connectivity between the rock surface and electrodes. Establishing a reliable procedure for resistivity measurements involving high sample and contact resistances would increase the information available about the electrical properties of rocks by allowing electrical

tomography of various rocks under various conditions.

There are some general requirements for the stable electrical measurement of rocks with multiple small electrodes under various conditions. First, the intensity of current injection must be kept constant. Second, the voltage must be measured precisely. Satisfying these two requirements is not easy, especially for high sample and contact resistances; therefore, a specific, optimised, experimental set-up is required. Third, the measurement environment must be precisely controlled. Electrical measurements of rocks are possibly affected by atmospheric humidity when conducted at ambient temperature and pressure; indeed, Okuyama (1972) and Alvarez (1973) reported that the resistance and resistivity of dry rock change greatly with the surrounding moisture conditions. With regard to the response of minerals to humidity, Soffer and Folman (1966), Colomer and Anderson (2001), and Umezawa et al. (2018) reported variations in the electrical conductivity of silica gel and silica nanoparticles with changing humidity.

This study aimed to develop a reliable procedure for stable multi-point electrical measurements on a rock sample with high contact resistance. To make the procedure

compatible with as wide a range of measurement conditions as possible, the designed method was applied to an extreme experimental condition; that is measuring dry rock at ambient temperature (about 300 K) and pressure (about 100 kPa), under which the contact and sample resistances are particularly high.

The remainder of this paper is organised as follows. Section 2 enumerates the requirements for stable multi-point electrical measurements on a rock sample with high contact resistance. Section 3 proposes a measurement procedure that fulfils these requirements. Section 4 describes the experimental set-up to test the method's performance. Section 5 assesses the stability and validity of the measured values and demonstrates the efficiency of the proposed procedure. Section 6 examines electrical measurements of a dry granite sample with many electrodes in a simple configuration as the first step toward electrical tomography. Section 7 presents the conclusions.

2. Measurement Requirements

Stable electrical measurements with small electrodes on rock samples against high sample and contact resistance have the following requirements regarding the electrodes,

current sources, voltmeters, noise reduction, and measurement environment.

(1) Electrodes

The measurement electrodes should be strongly attached with high conductivity, even when electrodes of arbitrary shape are used on the surfaces of dry rocks. Previous studies have employed metal plate electrodes of silver, molybdenum, or brass (e.g., Collett 1959; Fuji-ta et al. 2004; Borsic et al. 2005). However, metal plates do not contact the sample unless the sample surface is sufficiently wet or under confining pressure. Even in experiments with wet samples, a porous filter paper is often placed between the wet sample and electrode to connect them with the fluid. It is necessary for electrodes to be attachable to dry rocks at room temperature and pressure.

(2) Current injection

Electrical current must be injected into a high-resistance rock for a long period during measurement. Previous studies have employed function generators for current injection (e.g., Fuji-ta et al. 2004). However, common function generators are incompatible with very-high-resistance samples due to difficulties in applying high voltage and controlling the micro-current.

(3) Voltage measurement

The voltage across a dry, high-resistance rock should be measured accurately. The conventional multimeters used in previous studies are not suitable for measuring voltage at high resistance (over about 10 GΩ) due to their low internal resistance. The voltmeter must have an internal resistance far greater than the target resistance.

(4) Noise reduction

The measurement procedure should be designed to reduce expected noise in measurements at high resistance. This includes noise from the power supply, because even minute variations in the current have a large effect, owing to the injected current being very small in a high-resistance sample. Current leakage from insulation in the measurement circuit needs to be prevented. In high-resistance measurements, if the insulation and samples have similar resistance, then injected current would flow through both.

(5) Measurement environment

High-resistance measurement also requires a stable measurement environment with little variation in temperature, humidity, and other environmental conditions. As the

current flow is very low, changes in the measurement environment can significantly affect measurements.

3. Proposed measurement procedure

The current-injection and voltage-measurement techniques described here address the problems enumerated in the previous section regarding stable multi-point electrical measurements against high resistance.

(1) Electrodes

Favourable properties in the measuring electrodes are achieved through using a conductive adhesive comprising uniformly dispersed conductive particles (e.g., silver) in an epoxy resin organic binder. The conductive adhesive allows arbitrary arrangements and shapes of the electrodes. Furthermore, it provides stable attachment for all surface types.

(2) Current injection

To achieve current injection at high resistance, the system for current injection and voltage measurement is designed as shown in Fig. 1; it is compared alongside a

conventional measuring circuit. Our method uses a constant direct current source with high internal resistance in the same manner as Yamashita et al. (2014). There are two ways of finding resistance: measuring current under constant applied voltage and measuring voltage under constant current. For very-high resistance samples, the constant-current method generates large voltage signals that provide more accurate results than the very small currents recorded under constant voltage. Direct current (DC) was selected here for its suitability for high-resistance measurements, which arises for the following reasons. First, applying alternating current (AC) to a high-resistance sample that exceeds 1 GΩ is difficult and few instruments can facilitate this. Second, the transient response time of the measured value is not negligible for high-resistance measurements using AC. In contrast, using DC does not include these difficulties. In addition, it is not necessary to consider the influence of the skin effect in DC measurements. Therefore, we decided to use DC in our measurements.

(3) Voltage measurement

The proposed method ensures accurate voltage measurement by differential measurement using two voltmeters with high input resistance. In the resistance

measurement of dry rock, insulation resistance between the negative terminal and chassis ground may be smaller than the sum of the sample and contact resistance, allowing current to leak into the negative terminal of the voltmeter. Even using a voltmeter with high input resistance (as used by Yamashita et al. 2014), current can leak with the conventional four-terminal circuit shown in Fig. 1(A), because the insulation resistance is usually much smaller than the input resistance. This problem is solved by shorting the negative terminal of the high input resistance voltmeter to the negative terminal of the current source. However, this short circuit causes the measured voltage to include a voltage drop by the contact resistance of the negative current electrode and potential fluctuation at the signal ground of the current source. This study uses the differential measurement shown in Fig. 1(B) to eliminate the above effects. The difference between the outputs of the two voltmeters yields the potential difference, while the signals common to both voltmeters cancel.

(4) Noise reduction

The differential measurement circuit has the voltage common to the negative terminals separated from that of the chassis ground to remove noise from the power

supply. The guarding described by Tektronix (2016) is adopted to reduce current leakage from the measurement cables. It is applied to the wiring from the measurement instrument to the switch unit and sets the shield of the coaxial cable at the same potential as the inner conductor. When the shield is at the same potential as the inner conductor, there is no current flow between them. Therefore, this technique greatly reduces current leakage in the cable.

(5) Measurement environment

All measurements are performed with temperature and humidity kept as constant as possible using a humidifier, dehumidifier, and an air conditioner to reduce changes of sample resistance due to fluctuations in atmospheric moisture.

Human disturbance (e.g., vibration of the measurement circuit when attaching/detaching terminals and handling samples, and changes in temperature and humidity when staff enter or leave the laboratory) can cause strong signal noise; therefore, the proposed method employs remote operation of the instruments and a switching terminal to reduce signal noise arising from human activities.

4. Example of the experimental set-up

The performance of the proposed method was assessed in a test measurement using the sample, tools, and instruments described here.

The cylindrical granite measurement target (52 mm diameter, 100 mm length; white granite from China) used in the test is shown in Fig. 2(A). Its ends were ground parallel, and the surface was not polished. This study used granite as a measurement target, because it is a typical rock component of the upper crust. As we hope to apply our measuring procedure to electrical tomography using dozens of electrodes, our procedure should be evaluated using a relatively large sample capable of hosting many electrodes without overlap. To confirm the performance of the method applied to a sample with high contact and sample resistance, we used dried granite at ambient temperature and pressure.

(1) Electrodes

The electrodes were conductive epoxy adhesive (CW2400 Epoxy, Chemtronics, Mansfield, England). At any size it can be expected to have high adhesion and good conductivity, even on dry rock surfaces.

Before attaching the electrodes, the rock's cylindrical surface was masked by insulating masking tape, leaving gaps defining the electrode attachment area (Fig. 2(B) and (C)). This masking allowed precise control of the electrodes' positions. Copper wire was attached to the epoxy adhesive to connect the measurement instruments. Table 1 lists the physical properties of the conductive adhesive.

A small square electrode area of 100 mm^2 was used in this test of our new measurement method. As the procedure was designed for future use in electrical tomography, the performance needs to be assessed using small electrodes.

(2) Current injection

This study used two instruments to inject constant direct current depending on the experimental purposes. The first was an electrometer (Model 6514, Keithley, Cleveland, Ohio, US.). It was used in resistance measurement mode to inject direct constant current and measure the resulting voltage; resistance measurement is by two-terminal measurement. The measured resistance value is the sum of the sample resistance and contact resistance. The constant amount of injected direct current was set given the resistance range of the measured object (Table 2). The electrometer's maximum

measurable resistance was 210 GΩ. The experiments on the rock sample in Section 5 used an electrometer, because it was necessary to measure the two-terminal resistance, to separate out contact and sample resistance, and to evaluate the dependence of the measurement environment on the sample and contact resistance.

The other instrument to inject constant direct current was a direct-current voltage/current source monitor (Model 6243, ADC; Saitama, Japan), which was able to set the amount of injected direct current to an arbitrarily large value up to 2 A at up to 32 V. Its maximum applied voltage was 110 V, and the minimum resolution of the injected current was 1 nA. The experiments on plastic samples (Section 5) and rock (Section 6) used this device because they required the greatest injected current possible and increased signal-to-noise ratio in order to facilitate the measurement of potential distribution. The measurement of potential distribution required measurement of not only the potential near the current electrodes but also the low potential values far from them. Therefore, increased current was necessary to amplify the potential, and this required an instrument capable of setting the amount of injected current. The amount of injected current was measured by the ammeter of a multimeter (Model 3458A,

Keysight; Santa Rosa, California, USA) with 1 pA resolution.

(3) Voltage measurement

Voltage measurement was with an electrometer (Model 6514, Keithley, Cleveland, Ohio, USA) set to voltage measurement mode. This instrument was also used for differential measurements. Its negative terminal was shorted with the negative terminal of the current source. In voltage measurement mode, the maximum input resistance is 200 TΩ, and insulation resistance between the negative terminal and the chassis ground is 10 GΩ.

(4) Noise reduction

We electrically isolated the shorted negative terminal from the chassis ground to prevent the influence of ground noise. Each measuring instrument was connected to the power supply through the transformer to prevent noise from the outlet. In all the resistance and voltage measurements, guarding reduced leakage current.

(5) Measurement environment

Figure 3 shows the layout of the laboratory. The temperature in the laboratory was kept at 30 °C by an air conditioner during all measurements. Relative humidity was

controlled with a dehumidifier (Model DM-10; Nakatomi, Nagano, Japan) capable of setting humidity in the range 30%–90% in 5% steps and a humidifier (Model HD-152, Dainichi, Niigata, Japan) programmable to 60%, 70%, or 80% humidity. The humidity condition was maintained throughout the laboratory, except the very high humidity condition, which was maintained only inside the vinyl tent. Temperature and relative humidity were recorded hourly by a temperature and humidity logger (Model LR5001, Hioki, Ueda, Japan) placed near the granite sample. The granite sample, thermo-hygrometer, and switching unit were placed on the same desk, while the granite sample was placed on insulating rubber plates to prevent leakage current. The granite sample that was subjected to analyses is shown in Fig. 2(A).

Terminal switching was performed by the switch unit (HP34970A, Hewlett-Packard; Palo Alto, California, USA). All measurements were controlled by LabVIEW software (National Instruments, 15.0). Operators did not enter the laboratory during the measurement period.

5. Stability and validity of measurements

This section evaluates the stability and validity of the proposed measurement procedure.

We evaluated the stability of the procedure in terms of the stabilities of resistances measured between the current electrodes, R_{measured}, the potential difference measured between the potential electrodes, $V_{P_1} - V_{P_2}$, and the measured current, I. To evaluate the stabilities, we set six levels of relative humidity and constant temperature. At each level, we checked the stability through six sequences of repeated measurements.

In addition, we checked the adhesion performance through observations of the contact surface, because strong adhesion between electrodes and the sample is important in our experimental set-up.

5.1. Stability evaluation

5.1.1. Configuration of electrodes

Figure 4 shows the granite sample's cylindrical surface and the electrode arrangement with the measurement instruments. We observed the contact surface by micro-focus X-ray computed tomography (CT) to confirm the contact state of the electrodes. The CT results in Fig. 5 show that the electrodes were well attached, despite the roughness of

the surface, thus demonstrating the strong adhesion achieved by the proposed method.

5.1.2. Data sampling with humidity and temperature setting

R_{measured}, I, and $V_{P_1} - V_{P_2}$, were measured for 600 s in each measurement, which was repeated multiple times. Sampling was conducted every 1 s. To eliminate the charge between the current electrode and granite surface, all terminals were shorted after each 600 s measurement. The discharge time for each repeat measurement was set to 2 h during resistance measurements in the GΩ range. Resistance measurements in the MΩ range used a longer discharge time of 6 h due to the greater injected current amount (Table 2).

Six sequences of repeated measurements gathered data for R_{measured}, I, and $V_{P_1} - V_{P_2}$. One sequence is considered as a group of repeated measurement data performed at fixed humidity and temperature. The six sequences considered relative humidity at six set values (40%, 50%, 60%, 70%, 80%, and 90%) and constant temperature (30 °C).

5.1.3. Procedure for separating sample and contact resistance from measured resistance

The R_{measured} obtained by two-terminal measurement includes the sample resistance

between the current electrodes, R_{sample}, and the contact resistance between the electrodes, R_{contact}. We separate R_{measured} into R_{sample} and R_{contact} by the following procedure.

First, we determine the sample resistivity, ρ_{sample}, using I and $V_{\text{P}_1} - V_{\text{P}_2}$. We assume that the sample is homogeneous and isotropic. When the current I is injected through the current electrode, the potential difference $V_{\text{P}_1} - V_{\text{P}_2}$ is expressed as

$$V_{\text{P}_1} - V_{\text{P}_2} = \rho_{\text{sample}} K(\text{P}_1, \text{P}_2) I, \qquad (1)$$

where K is a function of the positions of a pair of potential electrodes. In general, the function K is determined either by solving the boundary value problem for the potential distribution or experimentally for a given shape of the conductive medium and the given positions of current electrodes. This work determines K using a numerical calculation code developed by Suzuki et al. (2017), which is a modified version of the classical procedure proposed by Dey and Morrison (1979) for cylindrical coordinates.

Here, the unknown ρ_{sample} is determined to fit the measured I, $V_{\text{P}_1} - V_{\text{P}_2}$, and the determined K. Once ρ_{sample} is found, the potential difference between current electrodes $V_{\text{C}_1} - V_{\text{C}_2}$ is calculated:

$$V_{C_1} - V_{C_2} = \rho_{\text{sample}} K(C_1, C_2) I, \qquad (2)$$

which implies that the resistance between the current electrodes, R_{sample}, is given by

$$R_{\text{sample}} = \frac{V_{C_1} - V_{C_2}}{I} = \rho_{\text{sample}} K(C_1, C_2). \qquad (3)$$

The contact resistance R_{contact} can then be determined. The resistance R_{measured} obtained by the two-terminal measurements is not the same as R_{sample} but the sum of R_{contact} and R_{sample}. Note that the contact resistance R_{contact} affects neither the calculated $V_{C_1} - V_{C_2}$ nor I; thus, R_{contact} does not affect R_{sample} in Eq. 3. Assuming that the contact resistances R_{contact} at both current electrodes are the same, R_{contact} is determined by

$$R_{\text{measured}} = R_{\text{sample}} + 2R_{\text{contact}}. \qquad (4)$$

This procedure for separating sample and contact resistance from measured resistance is shown in Fig. 6. Note that the electrode arrangement shown is that adopted in this study, and our procedure can separate sample and contact resistance from measured resistance in any electrode arrangement.

5.1.4. Inspection and processing of time-series data

The stability of the measured resistance, current, and potential difference was assessed using time series of the data of the type depicted in Fig. 7 for 40% relative

humidity and 30 °C. The time-series data show transient phenomena. The current recorded for about 1 min after the start of measurement was larger than that specified by the resistance meter (0.9 nA; Table 2). This large current meant that it took several tens of seconds for the measured resistance and potential difference to stabilise.

The large current at the start of measurement was interpreted as an inrush current. The increase of observed resistance after the current had settled probably corresponds to charging. Both of these effects shifted the measured resistance to higher values than their actual values. Therefore, it is reasonable to adopt the minimum value observed in each 600 s of resistance data, which likely includes the smallest effects of charging and inrush current.

On the other hand, after the inrush current, the current and potential difference became almost constant in the time-series data, making the data points equivalent. For standardised selection, the current and potential difference at the time of minimum resistance were chosen, as indicated by the dashed line in Fig. 7.

5.1.5. Stability of repeated measurements

Table 3 shows the stability of temperature, relative humidity, and absolute humidity

in the six sequences. In each case, temperature varied by at most approximately 0.5 °C, and humidity varied by at most approximately 3%. The measured temperature and humidity were far more stable than those of the outside air.

Figure 8 and Table 4 show the results of repeated measurements in the six sequences and their statistical comparison, respectively. Figure 8(A) confirms that the specified current of 0.9 nA was injected correctly without leakage current. Figure 8(B) and (C) shows the high stability and reproducibility of measurement. Because the current flowing through the ammeter is the sum of the injected current and the noise current, the observed current is larger than the specified current of 0.9 nA. We defined the fluctuation at each sequence as the standard deviation of all measurements in each sequence. The potential differences and resistances considerably decreased with increasing absolute humidity, with measured resistance being especially sensitive to absolute humidity even within each sequence.

The stability of the four-terminal measurement was assessed using standard deviations of the potential difference between potential electrodes $P_1 - P_2$ and of the intensity of the injected current. That of the two-terminal measurement was assessed

using the standard deviation of the resistance measured at each humidity setting. Table 4 lists these statistics, together with averaged values of corresponding quantities. From the listed values and the results of forward modelling, we estimated ρ_{sample} as listed in Table 5 by means of the procedure explained in Section 5.1.3. This estimation excluded negative values of the potential difference between P_1 and P_2 that appeared at humidity settings of 70% and 80%, because potential differences between these electrodes must be positive, and thus a negative value implies some problem with the measurement. The standard deviations of estimated resistivity were small compared with their mean values, indicating the stability of the obtained ρ_{sample}. Note that the order of obtained resistivity (between 10^5 and 10^6 Ω・m) at humidity between 50% and 80% was consistent with the bulk resistivity values of dry granodiorite reported in Chiba and Kumada (1994).

5.1.6. Estimation of resistance between current electrodes and contact resistance

Figure 9 shows estimated values for R_{sample} and $R_{contact}$. Not only R_{sample}, but also $R_{contact}$, greatly decreased with increasing absolute humidity, further showing the necessity of controlling humidity in the laboratory for measurements of dry rock

resistance.

$R_{contact}$ was much larger than R_{sample}, and accounted for most of each $R_{measured}$ value in Fig. 8(C). This suggests that the area of the current path present on the electrode bonding surface is small with respect to the apparent electrode size: current appears to flow between the rock surface and the electrode only through part of the contact area observed by CT scanning.

Changes in R_{sample} and ρ_{sample} with changes in humidity were attributed to moisture absorption by the sample. Alvarez (1973) and Okuyama (1972) reported that moisture greatly changes the resistance and resistivity of dry rock. Alvarez (1973) concluded that the adsorption of water molecules to minerals changed the resistance of rock samples, as also suggested by the present results.

The resistivity obtained here is that of a rock considered an aggregate of minerals. Although a surface water film on the nm scale or thinner can also affect the resistivity, surface conduction in the electric double layer is considered negligible here, because our experiments were performed at low humidity. Previous studies (e.g., Gee et al., 1990; Mazzoco and Wayner, 1999; Pashley and Kitchener, 1979) have found the water

film on a quartz surface to be several nm thick at around 95% relative humidity. As our experiments were performed at lower humidity conditions, the water film thickness in our measurements was considered to be several nm or less. In this case, unless the ion concentration of water in the atmosphere is extremely high, it is not necessary to consider the effect of the electric double layer. The observed high resistivity and resistance of our rock sample is consistent with this proposition.

We interpret the changes in R_{contact} to reflect atmospheric moisture penetrating the contact surface and filling minute gaps between the electrode and rock surface, thus increasing the contact points. It is reasonable to assume that moisture adsorption would occur even at the contact surface. Linear fitting to the estimated results (Fig. 9) is used to investigate whether the relationship between absolute humidity and R_{contact} can be expressed by a simple function. The estimated R_{contact} appears mostly consistent with the fitting results, which implies the presence of an exponential relationship between absolute humidity and R_{contact}. The observed exponential relationship suggests that the number of contact points on the contact surface changes exponentially with changes in humidity. The fitting function assumes an exponential relationship for $R_{\mathrm{contact}} = C10^{aH_A}$,

where C and a are constants, and H_A is absolute humidity.

5.2. Validity evaluation

To check the validity of the procedure for estimating the sample resistivity described in Section 5.1.3, we applied the method to plastic samples of known resistivity. We processed each type of plastic into a cylinder and a thin disk. The resistivity of the thin disk was determined by bulk resistivity measurement and that of the cylinder was determined by our method. The obtained resistivity values, together with the supplier's nominal resistivity value, were compared.

We used two types of plastics with different resistivity, one low (MC501CD R2, Mitsubishi Chemical Advanced Materials, Tokyo, Japan) and the other high (MC500AS R11, Mitsubishi Chemical Advanced Materials, Tokyo, Japan). Figure 10 shows photographs of the samples. Their nominal resistivity values are 10^0 to 10^2 Ω・m and 10^8 to 10^{10} Ω・m, respectively (Mitsubishi Chemical Advanced Materials, 2020a, b). Each was cut into a cylinder and thin disk (Fig. 10 (A-1), (A-2), (B-1), and (B-2)). For the thin disk, current electrodes made of conductive epoxy were attached to both ends and potential electrodes made of wire were attached to the side surface (Fig. 10 (A-3)

and (B-3)). This bulk resistivity measurement set-up is the same as that of Collet (1959) and Chiba and Kumada (1994). On the other hand, each cylinder had multiple small electrodes attached to its side surface for measurement by our proposed procedure. Figure 11 shows the side surface of the plastic cylinder and the electrode arrangement with the measurement instruments. This set-up was the same as that for the rock sample.

The resistivities of CD R2 and AS R11 were determined by bulk resistivity measurement to be 2.48 Ω・m and 1.50×10^7 Ω・m, respectively. Tables 6 and 7 list the results from our procedure. For both samples, the results from both methods were generally consistent both with each other and with the nominal values. The determined resistivity of AS R11 was an order of magnitude lower than the lower limit of the nominal range. The deviation was attributed to product error because values obtained by both measurement methods matched each other.

These results confirm that ρ_{sample} can be correctly estimated by our procedure for both high- and low-resistivity samples, thus demonstrating the validity of our procedure. They also confirm that our method can correctly estimate ρ_{sample}, regardless of the electrode arrangement.

6. Electrical measurements using an electrode array

We performed electrical measurements on intact rock using many electrodes in a simple configuration as a first step toward electrical tomography measurements. A constant current was injected into the sample, and the resulting potential distribution on the sample's cylindrical surface was measured using an electrode array. Sample resistivity, ρ_{sample}, was determined using numerical calculation with the measured potential distribution and current.

6.1. Measurement procedure

6.1.1. Measurement set-up and procedure

Figure 12 shows a photograph and a schematic diagram of the cylindrical surface of the granite sample on which 40 electrodes were arranged.

During measurement, a constant direct current was injected. The electrical potential of each potential electrode was measured via terminal switching. The positive terminal of V_1 was switched among the electrodes by the switch unit, whereas that of V_2 was fixed during measurement (Fig. 12(B)). Sampling was every 1 s. Electrical potential

was measured for 600 s for each potential electrode. From this measurement, the potential distribution relative to the potential of the electrode connected to V_2 was obtained. The potential was ignored for the first 5400 s from the start of the current injection to avoid the effect of the inrush current. At the end of the sequence, we re-measured the potential at an electrode previously assessed at the beginning of the sequence to confirm that the potential did not temporally change. During the measurement, the temperature was kept at about 30 °C, and the relative humidity was kept at about 70%; therefore, the absolute humidity was kept at about 21.7 g/m^3.

6.1.2. Procedure for determining sample resistivity using the measured potential distribution

Based on the measured values of potential differences and current intensity, we determined ρ_{sample} by the procedure described in Section 5.1.3. The stability test in Sections 5.1.5 and 5.1.6 determined ρ_{sample} and R_{sample} only using one potential difference between one pair of potential electrodes, but here ρ_{sample} and R_{sample} are determined from the potential distribution obtained from 38 electrodes. The modelling assumed the medium to have homogeneous and isotropic resistivity. Because the array

measurement requires a relatively long time (30,000 s) for each sequence, the intensity of the injected current involved minor fluctuations, although we tried to maintain a constant current of 100 nA. The effect of this in the measured potential must be considered when comparing the results with those of numerical calculations with fixed current intensity. Therefore, we normalised the measured potential $V_{\text{uncorrected}}$ to $V_{\text{corrected}}$ = $V_{\text{uncorrected}} \frac{(100\ \text{nA})}{I}$ and regarded it as the measured value. The value of ρ_{sample} was determined so that it minimised the total difference between the measured and calculated potential at 38 potential electrodes, excluding the current electrodes by the following procedure. Here, equation (1) is equivalent to

$$V_i - V_{(Z1,\theta 4)} = \rho_{\text{sample}} K\big(i, (Z1, \theta 4)\big) I + V_{\text{offset}}. \qquad (5)$$

V_i is the electrical potential at the potential electrode at point i measured via terminal switching. $V_{(Z1,\,\theta 4)}$ is the electrical potential at the potential electrode at point ($Z1$, $\theta 4$). The constant V_{offset} represents the difference between the actual and calculated potentials at the reference point $(Z1, \theta 4)$. K is determined as in Section 5.1.3. Two unknowns, ρ_{sample} and V_{offset}, are determined to fit the measured I and $V_i - V_{(Z1,\theta 4)}$ by least squares.

6.2. Results and Discussion

6.2.1 Inspection and processing of time-series data

Figure 13 (A-1) to (E-1) shows the potentials obtained in each *z*-line indicated in Fig. 12 (A) and (B). The V_{offset} determined in Section 5.1.3 was removed from the measurement values shown in Fig. 13. At each point, data obtained at seven timings (i.e., 60, 100, 200, 300, 400, 500, and 600 s) in the 600 s time-series were plotted: their invariance confirms the stability of the time-series data after the inrush current; nevertheless, we used the average of the last 100 s of the 600 s of data, as the end of the time-series is expected to have the least noise due to terminal switching. The current measurement similarly used the average of the last 100 s of the 600 s of data.

6.2.2. Obtained potential distribution and modelling results

Comparison of the measured potentials and the results of forward modelling with the optimum value of ρ_{sample} is shown in Fig. 13 (A-2) to (E-2). All *z* lines showed consistent measured and calculated potentials, indicating the validity of the measurement.

In addition, the resistivity obtained with the electrode array was consistent with the results of repeated measurements in six sequences when considering the effect of

humidity. The resistivity determined with the electrode array was 6.7×10^5 Ω・m. The repeated measurements at relatively high humidity were performed at 20.3 ± 0.5 and 23.6 ± 0.7 g/m^3 absolute humidity, whereas the array measurement was performed at 21.7 g/m^3 absolute humidity, which is between the two values of the repeated measurements. The corresponding resistivities determined in the repeated measurements were $(1.7 \pm 0.4) \times 10^6$ and $(1.4 \pm 1.0) \times 10^5$ Ω・m, respectively, and that determined by the array measurement fell between them, as expected given the humidity dependency of resistivity.

The array measurement will be applied to electrical tomography in combination with an inversion process. Electrical tomography has previously been considered possible only under restricted conditions such as high water-saturation (Stacey, 2006). However, the present results for dry rock demonstrate that our procedure can facilitate tomographic measurements for a variety of targets under wider conditions than considered previously.

An interesting measurement target is one containing fractures. Compression tests of granite samples of the same size as used here have been widely performed, and to

prepare samples with heterogeneous structures is not difficult. Comparison of electrical and CT measurement results may provide useful information about the electrical properties of heterogeneous structures. Previous studies have used CT imaging to investigate fracture distributions in granite samples (e.g., Kawakata et al. 1999).

7. Conclusions

We propose a reliable procedure for stable multi-point electrical measurements on a rock sample with high contact resistance. The method employs conductive epoxy adhesive electrodes to achieve secure attachment and high conduction on a dry rock surface. Stable current was injected into high-resistance samples using a constant direct current source with high internal resistance. Voltage was accurately measured in high-resistance samples via differential measurement with two high input resistance voltmeters. The problem of leakage current through the negative terminal of the voltmeter was solved by shorting it to the negative terminal of the current source. Contact resistance and potential fluctuation in the negative current electrode were eliminated by the differential measurement. Temperature and humidity in the laboratory

were controlled using a humidifier, a dehumidifier, and a vinyl tent. Potential sources of signal noise from human activity were eliminated by using remote terminal switching and instrument operation.

We applied the new method to dry granite samples and evaluated its precision and stability under multiple absolute humidity conditions. At each humidity, the measurements were highly reproducible, thus indicating the stability of our new method. Nonetheless, atmospheric moisture did greatly influence the sample resistance and contact resistance, showing that humidity, alongside temperature, is an important environmental factor that must be controlled in the laboratory. Very high resistance exceeding 100 GΩ can be measured repeatedly by the new method even while using a small 100 mm^2 electrode. We also applied the new method to multiple plastic samples of known resistivity to confirm the consistency of its resistivity results with bulk resistivity measurements.

We performed electrical measurements on a dry granite sample using many electrodes as the first step toward electrical tomography. The potential distribution calculated by forward modelling was consistent with the measured distribution,

indicating the robustness of the measurement procedure and its potential capability for electrical tomography on high-resistance rock samples with high contact resistance (e.g., dry rocks). We also confirmed that the determined resistivity varied as expected with changing humidity.

List of abbreviations

H_A: absolute humidity

$R_{measured}$: resistance measured between the current electrodes

R_{sample}: sample resistance between the current electrodes

$R_{contact}$: contact resistance at the electrodes

R_{IN}: input resistance

R_V: insulation resistance between the negative terminal and chassis ground

V_{offset}: difference between the actual and calculated potentials at the reference point $(Z1, \theta4)$

$V_{P_1} - V_{P_2}$: potential difference between the potential electrodes

$V_{C_1} - V_{C_2}$: potential difference between the current electrodes

$V_{uncorrected}$: Potential difference uncorrected for fluctuations in injection current intensity in array measurement

$V_{corrected}$: Potential difference corrected for fluctuations in injection current intensity in array measurement

ρ_{sample}: sample resistivity

I: injected current

Declarations

Availability of data and materials

The data that support the findings of this study are available upon request from the corresponding author.

Competing interests

The authors declare that they have no competing interests.

Funding

This study was partially funded by the New Exploratory Research (28H-

02, 29H-04) at the Disaster Prevention Research Institute, Kyoto University.

Authors' contributions

TS developed the measurement method, applied the method to samples, interpreted the obtained results, led the discussion, and wrote the first draft of the manuscript. RY, KY, and NO contributed to analysis and interpretation of data, and assisted in the preparation of the manuscript. All authors revised and improved the manuscript. All authors read and approved the final manuscript.

Acknowledgements

We thank the National Research Institute for Earth Science and Disaster Resilience and the Research Institute for Sustainable Humanosphere, Kyoto University for providing the measurement equipment used in this study. Futoshi Yamashita, Hironori Kawakata, and Yasuyuki Kano are thanked for their help at the early stage of this study. We also thank Takuto Minami, Ryousuke Umezawa, Shinichi Takakura, and

anonymous reviewers for valuable comments that improved an earlier version of the manuscript. Micro-focus X-ray CT measurements were performed under the cooperative research program (number 18B057) of the Center for Advanced Marine Core Research (CMCR), Kochi University. We thank Yuji Yamamoto, Masafumi Murayama, and Takuya Matsuzaki for technical support with the micro-focus X-ray CT measurements.

Authors' information

1 Graduate School of Science, Kyoto University, Gokasho, Uji, Kyoto 611-0011, Japan. 2 Disaster Prevention Research Institute, Kyoto University, Gokasho, Uji. Kyoto 611-0011, Japan. 3 Miyazaki Observatory, Research Center for Earthquake Prediction, Disaster Prevention Research Institute, Kyoto University, 3884, Kaeda, Miyazaki 889-2161, Japan.

Consent for publication

Not applicable.

Ethics approval and consent to participate

Not applicable.

References

Alvarez R (1973) Effects of atmospheric moisture on rock resistivity. J Geophys Res 78(11):1769-1779.

Borsic A, Comina C, Foti S, Lancellotta R, Musso G (2005) Imaging heterogeneities with electrical impedance tomography: laboratory results. Géotechnique 55(7):539-547.

Brace WF, Orange AS, Madden, TR (1965) The effect of pressure on the electrical resistivity of water-saturated crystalline rocks. J Geophys Res 70(22):5669–5678.

Chiba A, Kumada M (1994) Resistivity measurement for granite and tuff samples - influence of pore fluid resistivity on rock resistivity. Butsuri-Tansa 47(4):161–172 (In Japanese with English abstract).

Collet LS (1959) Laboratory investigation of overvoltage. In: Wait JR (ed) Overvoltage research and geophysical applications. Pergamon Press, Oxford, pp 50–60.

Colomer MT, Anderson MA (2001) High porosity silica xerogels prepared by a particulate sol–gel route: pore structure and proton conductivity. Journal of Non-Crystalline Solids 290(2–3):93–104.

Coster HP (1948) The electrical conductivity of rocks at high temperatures. Geophys J Int 5:193–199.

Dey A, Morrison HF (1979) Resistivity modeling for arbitrarily shaped three-dimensional structures. Geophysics 44(4):753-780.

Fuji-ta K, Katsura T, Tainosho Y (2004) Electrical conductivity measurement of granulite under mid-to lower crustal pressure—temperature conditions. Geophys J Int

157(1):79-86.

Fuji-ta K, Katsura T, Matsuzaki T, Ichiki M, and Kobayashi T (2007) Electrical conductivity measurement of gneiss under mid-to-lower crustal P–T conditions. Tectonophys 434(1-4):93-101.

Gee ML, Healy TW, White LR (1990) Hydrophobicity effects in the condensation of water films on quartz. Journal of Colloid and Interface Science 140:450–46.

Kariya KA, Shankland TJ (1983) Electrical conductivity of dry lower crustal rocks. Geophys 48(1):52-61

Kawakata H, Cho A, Kiyama T, Yanagidani T, Kusunose K, Shimada M (1999) Three-dimensional observations of faulting process in Westerly granite under uniaxial and triaxial conditions by X-ray CT scan. Tectonophysics 313(3):293–305.

Mazzoco RR, Wayner Jr PC (1999) Aqueous wetting films on fused quartz. Journal of Colloid and Interface Science 214:156–169.

Mitsubishi Chemical Advanced Materials (2020a) MC Nylon MC501CD R2 (electro conductive grade). https://www.mcam.com/jp-en/products/engineering-plastics/engineering-80-160/extruded-cast-nylons/mc501cd-r2/. Accessed 31 Dec 2020

Mitsubishi Chemical Advanced Materials (2020b) MC Nylon MC500AS R11 (noncarbon antistatic grade). https://www.mcam.com/jp-en/products/engineering-plastics/engineering-80-160/extruded-cast-nylons/mc500as-r11/. Accessed 31 Dec 2020

Okuyama Y (1973) The effects of water content on the electrical resistivity of rocks. Bull Akita Natl Coll Technol 8:110-114 (In Japanese).

Pashley RM, Kitchener JA (1979) Surface forces in adsorbed multilayers of water on quartz. Journal of Colloid and Interface Science 71:491–500

Soffer A, Folman M (1966) Surface conductivity and conduction mechanisms on adsorption of vapours on silica. Transactions of the Faraday Society 62:3559–3569.

Suzuki T, Yoshimura R, Yamazaki K, Oshiman N (2017) Potential modeling for cylindrical shaped structures. Disaster Prevent Res Inst Annu B (2017) 60(b):373-281 (In Japanese with English abstract).

Stacey R (2006) Electrical impedance tomography. Geothermal Program Interdisciplinary Research in Engineering and Earth Sciences. In Tech Rep SGP-TR-182. Stanford University.

Tektronix (2016) Low level measurements handbook, 7th edn. Tektronix, Beaverton

Umezawa R, Katsura M, Nakashima S (2018) Electrical conductivity at surfaces of silica nanoparticles with adsorbed water at various relative humidities. e-Journal of

Surface Science and Nanotechnology 16:376–381.

Yamashita F, Fukuyama E, Mizoguchi K (2014) Probing the slip-weakening mechanism of earthquakes with electrical conductivity: Rapid transition from asperity contact to gouge comminution. Geophys Res Lett 41(2):341-347.

Figure legends

Fig. 1

Circuitry of (A) the conventional four-terminal method and (B) the differential measurement method adopted here. The circled arrow is the direct current source, V and V_1 and V_2 are voltmeters, R_{IN} is input resistance, R_V is the insulation resistance between the negative terminal and chassis ground, R_{c2} is the contact resistance between the electrode and sample surface, and R_s is the sample resistance. HI labels positive terminals, LO labels negative terminals, C_1 and C_2 are current electrodes, P_1 and P_2 are potential electrodes. In (A) when the sum of R_{s3} and R_{c2} is much smaller than R_{IN} or R_V,

no current flows into the voltmeter. However, in a voltmeter, R_V is usually much smaller than R_{IN}. When R_V is less than the sum of R_{s3} and R_{c2}, current flows into R_V through the negative terminal of the voltmeter, preventing correct voltage measurement. In (B), R_V does not contribute to the current path, and when R_{IN} is larger than the sum of R_{s3} and R_{c2}, most of the current does not flow to the voltmeter. The differential method uses two voltmeters, whose positive terminals are connected to P_1 and P_2, and whose negative terminals are shorted to the negative terminal of the current source. The voltage between P_1 and P_2 is obtained as the voltage difference between the measured values of V_1 and V_2.

Fig. 2

Photographs of set-up for measurement of a granite sample. (A) The unpolished, cylindrical rock sample (52 mm diameter, 100 mm length) overlaid with the dimensions r, θ, and z defining its coordinate axis. (B) The electrode attachment area as controlled by insulating masking tape. (C) Conductive epoxy adhesive attached to the rock surface as a high-conductivity electrode. A wire attached to the adhesive provided a connection

for measuring instruments.

Fig. 3

(A) Layout of measurement instrumentation and (B) photograph of the measurement system in the laboratory. Humidity was controlled using a dehumidifier and a humidifier. The vinyl tent was used only when making very high humidity conditions, otherwise each condition was maintained throughout the laboratory. A thermo-hygrometer placed near the sample recorded temperature and humidity. The granite sample, thermo-hygrometer, and switching unit were placed on the same desk. All repeated measurements were performed without direct human intervention, because manual terminal switching and instrument operation would cause serious signal noise. The switching unit performed the connection of terminals and electrodes during repeated measurements. The instruments and switching unit were controlled using LabVIEW software on the PC.

Fig. 4

Measurement scheme. z and θ are coordinates defined in Fig. 2(A). The circled arrow is a direct current source, the dotted square is a resistance meter, V_1 and V_2 are voltmeters, A is an ammeter, R_{IN} is input resistance, R_V is insulation resistance between the negative terminal and chassis ground, HI labels positive terminals, LO labels negative terminals, C_1 and C_2 are current electrodes, and P_1 and P_2 are potential electrodes. In this study, a resistance meter was used as a direct current source. The resistance meter injects known direct constant current, measures the voltage caused by injected current, and obtains resistance. An ammeter (Model 3458A, Keysight; Santa Rosa, California, USA) was placed in order to monitor the amount of injected current. Electrometers (Model 6514, Keithley, Cleveland, Ohio, US.) with R_{IN} = 200 TΩ acted as the resistance meter and the voltmeter. Each measuring instrument was connected to the conductive epoxy adhesive used as electrodes shown in Fig. 2 (C).

Fig. 5

Microstructures of the contact surface observed by micro-focus X-ray computed tomography (CT). (A) Sample photograph showing the 100 mm^2 electrode. CT images

of the (B) *x–z* and (C) *x–y* planes; the pixel size is approximately 4 μm, and the scale bar in each image is 500 μm. Black in the CT images represents areas of X-ray transmission; the white areas are opaque to X-rays. Here, black represents mainly air, dark grey is mainly granite, and light grey is the conductive epoxy adhesive and wires. The images show roughness at the rock sample surface, and the good attachment of the electrodes to this rough surface.

Fig. 6

Estimation of resistance between current electrodes. The coordinates z and θ are as defined in Fig. 2(A). C_1 and C_2 are current electrodes, and P_1 and P_2 are potential electrodes. V_{C_1}, V_{C_2}, V_{P_1}, and V_{P_2} are electrical potential at C_1, C_2, P_1, and P_2. R_{measured}, R_{sample}, and R_{contact} are respectively the measured resistance between the current electrodes, the sample resistance between the current electrodes, and the contact resistance at the current electrodes. I is measured current. The left diagram depicts the measurement area (i.e., the sample's side surface), and the right diagram represents the numerical model of the measurement area with its calculation grids. Performing

numerical calculations under various sample resistivities searched for a potential distribution that mostly explains the observed $V_{P_1} - V_{P_2}$. The calculations assumed the sample to have a homogeneous resistivity structure. $V_{C_1} - V_{C_2}$ is extracted from the determined potential distribution, and used to obtain R_{sample} by dividing it by I.

Fig. 7

Representative time-series data for resistance, current, and potential difference. The results are those measured for 600 s at 40% relative humidity and 30°C using the measurement layout in Fig. 3. (A) Resistance between C_1 and C_2 measured by a resistance meter. (B) Current measured by an ammeter. (C) Potential difference between P_1 and P_2. The injected current took several tens of seconds to stabilise after measurement started. It was initially larger than the specified current used by the resistance meter to measure resistance in the GΩ range, and was interpreted as inrush current. This inrush current caused the resistance also to take several tens of seconds to stabilise, after which resistance increased. This was interpreted as charging. The minimum in the resistance data for 600 s is therefore considered the most representative

value, because the effects of inrush current and charging are likely smallest. Current and potential difference were taken as their values at the time when resistance was lowest, as indicated by the dashed line.

Fig. 8

Current, potential difference, and resistance with respect to absolute humidity. (A) Current measured by ammeter and (B) measured potential difference between P_1 and P_2 as a function of the absolute humidity. (C) Measured resistance between C_1 and C_2 as a function of the absolute humidity in log scale. Measurements were repeated in six sequences of relative humidity (40%, 50%, 60%, 70%, 80%, and 90%) under constant temperature (30 °C), with the symbols indicating the measurement sequence. Multiple measurements were performed for each sequence to confirm reproducibility. In each sequence, the minimum value observed in 600 s of resistance data was selected and plotted. The plotted current and potential difference are those at the time of minimum resistance. The injected current amount depended on the resistance measurement range (Table 2). The potential difference depended on the current amount difference. Dashed

lines indicate the boundary of the measurement range. Each sequence of repeated measurement results shows high repeatability.

Fig. 9

Estimated contact resistance and sample resistance with respect to absolute humidity. Resistances between current electrodes C_1 and C_2 are plotted as a function of the absolute humidity in log scale. The dashed line represents exponential fitting results, and the symbols indicate the measurement sequence. Sample resistance was estimated numerically from the measured current and potential difference values in Figs. 8(A) and (B). Contact resistance is half of the value obtained by subtracting the estimated sample resistance from the measured resistance value in Fig. 8(C). Both contact resistance and sample resistance decreased exponentially as the absolute humidity increased. Most of the resistance measured by the resistance meter appeared to be contact resistances. The relationship between contact resistance and absolute humidity was mostly represented by an exponential function.

Fig. 10

Photographs of set-up for measurement of plastic samples overlaid with the dimensions r, θ, and z defining the coordinate axis. Top row: Cylindrical plastic samples (A-1) MC501CD R2 (Mitsubishi Chemical Advanced Materials, Tokyo, Japan; 52 mm diameter, 100 mm length) and (B-1) MC500AS R11 (Mitsubishi Chemical Advanced Materials, Tokyo, Japan; 63 mm diameter, 100 mm length). Middle row: Thin-disk plastic samples (52 mm diameter, 30 length) of (A-2) MC501CD R2 and (B-2) MC500AS R11. Bottom row: Arrangement of wire potential electrodes around the thin-disk samples' side surface and conductive epoxy-adhesive current electrodes attached to their ends, (A-3) MC501CD R2 and (B-3) MC500AS R11.

Fig. 11

A scheme of measurement for the cylindrical plastic samples. z and θ are coordinates as defined in Fig. 10. The circled arrow is a constant DC source, V_1 and V_2 are voltmeters, A is an ammeter, R_{IN} is input resistance, R_V is insulation resistance between the negative terminal and chassis ground, HI labels positive terminals, LO labels negative terminals,

C_1 and C_2 are current electrodes, and P_1, P_2, P_3, P_4, P_5, and P_6 are potential electrodes. The DC source (Model 6243, ADC; Saitama, Japan) injected a known constant current. An ammeter (Model 3458A, Keysight; Santa Rosa, California, USA) monitored the injected current. Electrometers (Model 6514, Keithley, Cleveland, Ohio, US.) with R_{IN} = 200 TΩ acted as the voltmeters. Each measuring instrument was connected to the conductive epoxy adhesive used as electrodes shown in Fig. 2 (C).

Fig. 12

Photograph and schematic diagram of the measurement set-up with an array of electrodes. (A) Cylindrical rock sample (52 mm diameter and 100 mm length) overlaid with the dimensions r, θ, and z defining its coordinate axes. Electrodes were attached to the cylindrical surface, and wires attached to electrodes provided a connection for measuring instruments. (B) Measurement scheme. z and θ are coordinates defined in Fig. 10(A). The dotted square is a constant direct current source, V_1 and V_2 are voltmeters, A is an ammeter, R_{IN} is input resistance, R_V is insulation resistance between the negative terminal and chassis ground, HI labels positive terminals, and LO labels

negative terminals. The direct current source (Model 6243, ADC; Saitama, Japan) injected a known constant current. An ammeter (Model 3458A, Keysight; Santa Rosa, California, US.) monitored the amount of injected current. Electrometers (Model 6514, Keithley; Cleveland, Ohio, USA) with R_{IN} = 200 TΩ acted as the voltmeters. Each measuring instrument was connected to the conductive epoxy adhesive used as electrodes as shown in Fig. 2 (C).

Fig. 13

Profiles of electrical potential in the circumferential direction θ at each z from measurements using an electrode array. The coordinates z and θ are defined in Fig. 12. (A) Profile at $z1$ = 16.7 mm, (B) at $z2$ = 33.3mm, (C) at $z3$ = 50 mm, (D) at $z4$ = 66.7 mm, and (E) at $z5$ = 83.3 mm. Left panels (A-1 to E-1) show the measured value with elapsed time (60, 100, 200 s, etc.) from the start of the measurement at each potential electrode. The symbols indicate the data acquisition time. The reference point for the measured potential distribution used for comparison with the numerical results is the midpoint between the current electrodes. Right panels show numerical results of

forward modelling (A-2 to E-2). The orange and blue dots respectively indicate the experimental and numerical results. In experimental results, error bars are smaller than the symbols. Each measured value is the potential at each electrode averaged over the last 100 s of measurement. The numerical results were calculated by using the average of all 100 s current intensity data at the corresponding timing of potential observation. The measured values were normalised by the average current for comparison.

Tables

Table 1 Physical properties of conductive epoxy adhesive (Chemtronics CW2400)

Operating temperature range	−91 to 100 °C
Volume resistivity	< 10 μΩ·m
Main component	epoxy resin, silver, and hardener
Curing times	5–10 min from 65–121 °C, 4 h at or above 25 °C

Table 2 Accuracy specifications for resistance measurement by the electrometer

(Keithley 6514)

Range [Ω]	Resolution [Ω]	Direct injection current [A]
2×10^{6}	1×10^{1}	0.9×10^{-6}
2×10^{7}	1×10^{2}	0.9×10^{-6}
2×10^{8}	1×10^{3}	0.9×10^{-6}
2×10^{9}	1×10^{4}	0.9×10^{-9}
2×10^{10}	1×10^{5}	0.9×10^{-9}
2×10^{11}	1×10^{6}	0.9×10^{-9}

Table 3 Stability of temperature and relative humidity in each sequence

Humidity setting [%]	Mean and standard deviation			Number of recordings
	Temperature [°C]	Humidity [%]	Absolute humidity [g/m^3]	
40	29.4 ± 0.7	40.6 ± 2.1	11.9 ± 0.6	136
50	29.3 ± 0.3	51.1 ± 2.5	15.0 ± 0.6	67
60	29.3 ± 0.3	61.4 ± 1.6	17.9 ± 0.3	87
70	29.4 ± 0.4	69.2 ± 2.5	20.3 ± 0.5	80
80	29.5 ± 0.2	79.9 ± 2.5	23.6 ± 0.7	190
90	30.3 ± 0.3	89.2 ± 2.9	27.5 ± 0.8	117

Table 4 Statistical comparison of repeated measurements

Humidity setting [%]	Mean and standard deviation			Number of measurements
	Four-terminal measurement		Two-terminal measurement	
	Current [nA]	Potential difference [mV]	Resistance ($R_{measured}$) [Ω]	
40	1.06 ± 0.06	166.9 ± 14.4	$(1.36 \pm 0.02) \times 10^{11}$	6
50	1.03 ± 0.05	91.0 ± 23.2	$(5.27 \pm 0.97) \times 10^{10}$	33
60	1.05 ± 0.04	45.4 ± 12.8	$(1.36 \pm 0.62) \times 10^{10}$	43
70	1.06 ± 0.04	26.8 ± 11.0	$(3.20 \pm 1.48) \times 10^{9}$	39
80	1.09 ± 0.08	1.62 ± 5.94	$(1.86 \pm 1.20) \times 10^{8}$	94
90	937 ± 1	1152 ± 368	$(5.53 \pm 2.25) \times 10^{7}$	24

Note: The log quotient of potential difference and current in at 80% humidity is not calculable because the standard deviation of potential difference in the sequence is very large.

Table 5 Statistical comparison of estimated resistivity in repeated measurements

Humidity setting [%]	Mean and standard deviation		Number of estimated values
	Absolute humidity [g/m^3]	Estimated resistivity [Ω・m]	
40	11.9 ± 0.6	$(1.0 \pm 0.1) \times 10^7$	6
50	15.0 ± 0.6	$(5.7 \pm 1.4) \times 10^6$	33
60	17.9 ± 0.3	$(2.7 \pm 0.6) \times 10^6$	41
70	20.3 ± 0.5	$(1.7 \pm 0.4) \times 10^6$	38
80	23.6 ± 0.7	$(1.4 \pm 1.0) \times 10^5$	68
90	27.5 ± 0.8	$(7.6 \pm 2.0) \times 10^4$	23

Note: Any data outside the range of $(\text{mean}) \pm 3 \times (\text{standarddeviation})$ were removed as outliers, and the statistics were recalculated.

Table 6 Measurement results for the low-resistivity plastic sample (CD R2)

Sample	Pair of potential electrodes	Mean and standard deviation		Estimated sample resistivity [Ω・m]
		Injected current [mA]	Potential difference [V]	
CD R2	P_2–P_3	9.37 ± 0.01	0.517 ± 0.001	3.56
	P_5–P_3		0.246 ± 0.001	3.38
	P_4–P_1		0.259 ± 0.001	3.56
	P_4–P_6		0.211 ± 0.001	3.54

Table 7 Measurement results for the high-resistivity plastic sample (AS R11)

Sample	Pair of potential electrodes	Mean and standard deviation		Estimated sample resistivity [Ω・m]
		Injected current [nA]	Potential difference [V]	
AS R11	P_2–P_3	29.5 ± 0.1	6.64 ± 0.01	1.35×10^7
	P_5–P_3		3.15 ± 0.01	1.28×10^7
	P_4–P_1		3.28 ± 0.01	1.33×10^7
	P_4–P_6		2.45 ± 0.01	1.26×10^7

Figures

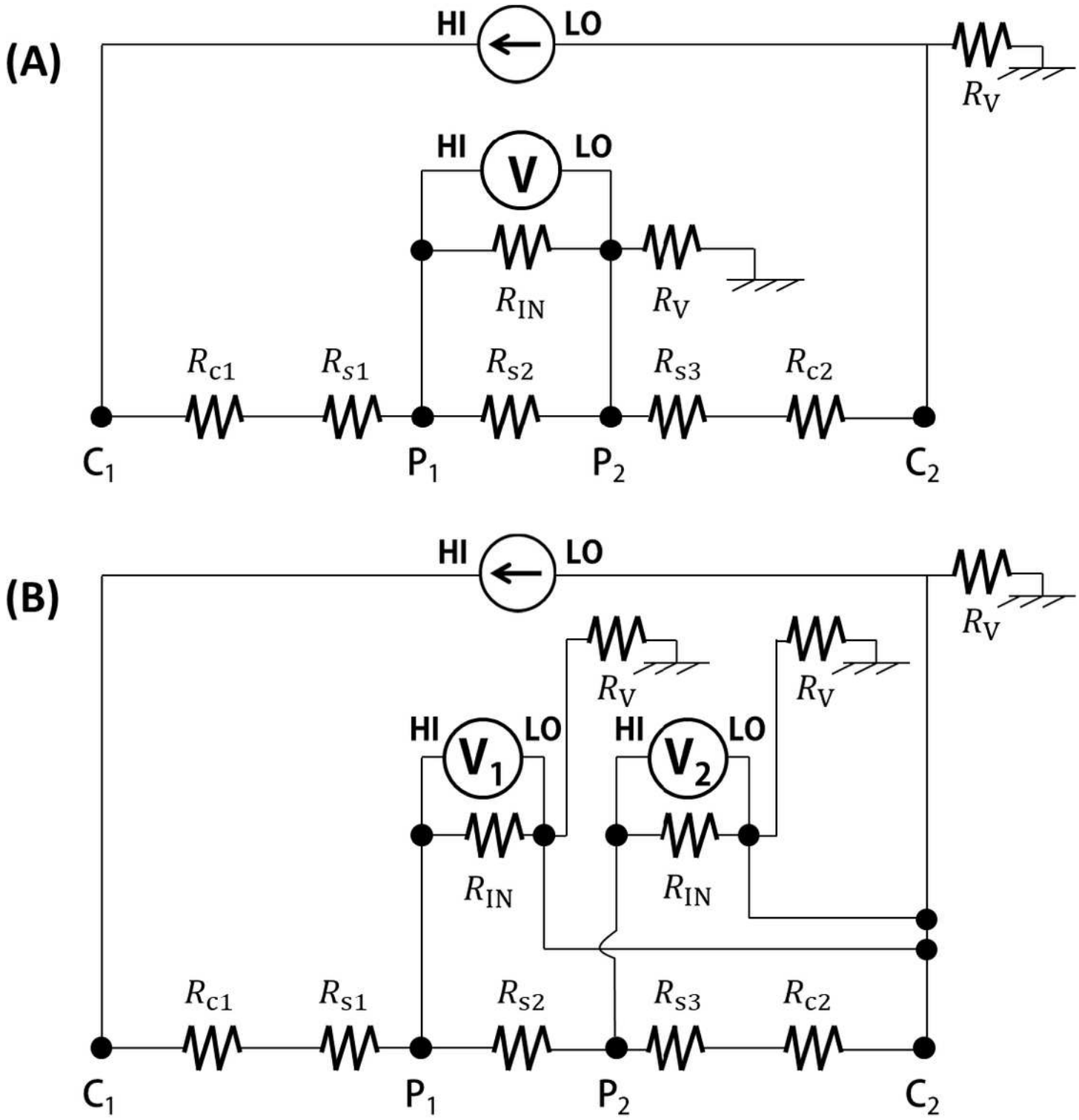

Figure 1

Circuitry of (A) the conventional four-terminal method and (B) the differential measurement method adopted here. The circled arrow is the direct current source, V and V1 and V2 are voltmeters, RIN is input resistance, RV is the insulation resistance between the negative terminal and chassis ground, Rc2 is the

contact resistance between the electrode and sample surface, and Rs is the sample resistance. HI labels positive terminals, LO labels negative terminals, C1 and C2 are current electrodes, P1 and P2 are potential electrodes. In (A) when the sum of Rs3 and Rc2 is much smaller than RIN or RV, no current flows into the voltmeter. However, in a voltmeter, RV is usually much smaller than RIN. When RV is less than the sum of Rs3 and Rc2, current flows into RV through the negative terminal of the voltmeter, preventing correct voltage measurement. In (B), RV does not contribute to the current path, and when RIN is larger than the sum of Rs3 and Rc2, most of the current does not flow to the voltmeter. The differential method uses two voltmeters, whose positive terminals are connected to P1 and P2, and whose negative terminals are shorted to the negative terminal of the current source. The voltage between P1 and P2 is obtained as the voltage difference between the measured values of V1 and V2.

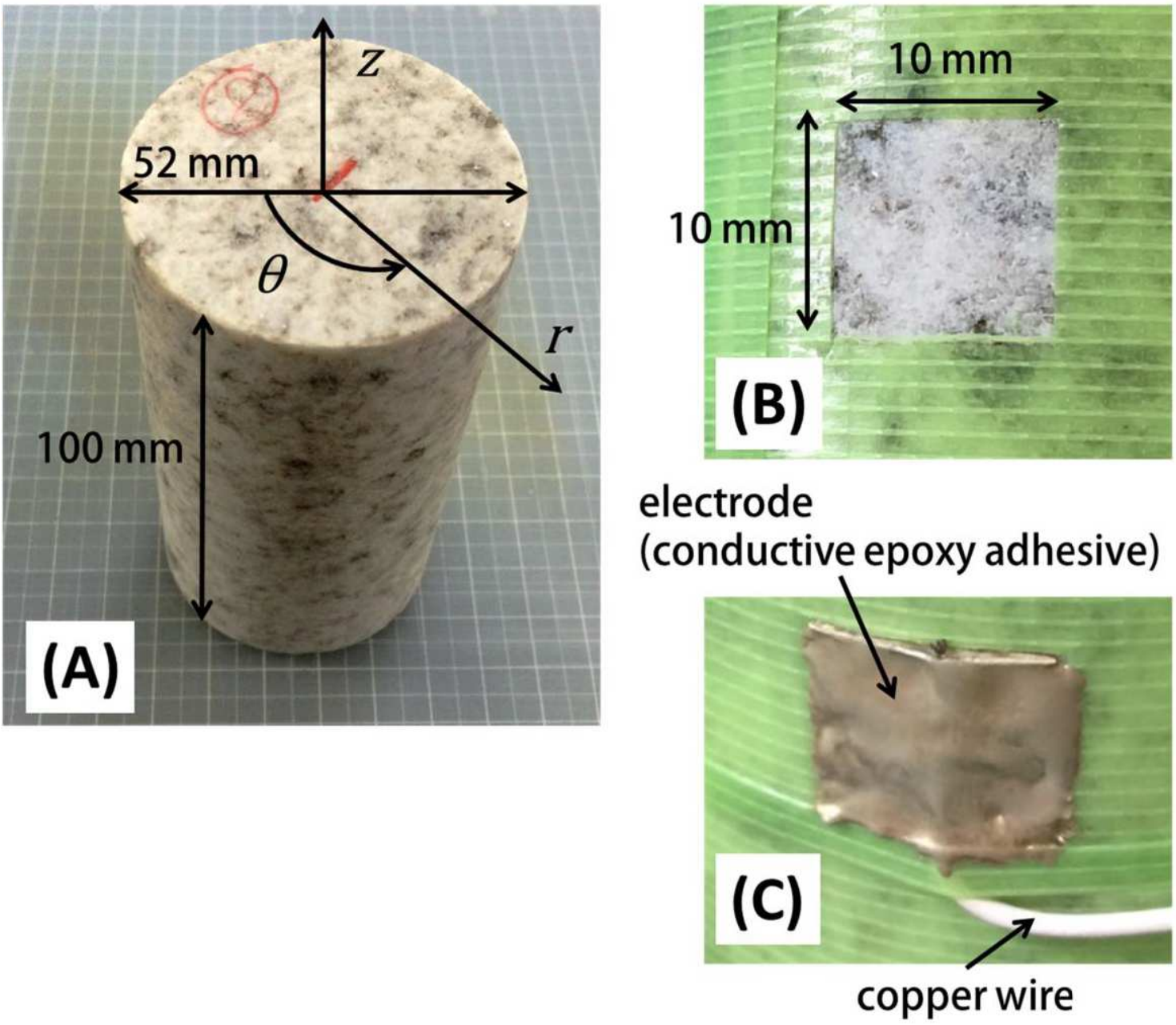

Figure 2

Photographs of set-up for measurement of a granite sample. (A) The unpolished, cylindrical rock sample (52 mm diameter, 100 mm length) overlaid with the dimensions r, θ, and z defining its coordinate axis. (B) The electrode attachment area as controlled by insulating masking tape. (C) Conductive epoxy adhesive attached to the rock surface as a high-conductivity electrode. A wire attached to the adhesive provided a connection for measuring instruments.

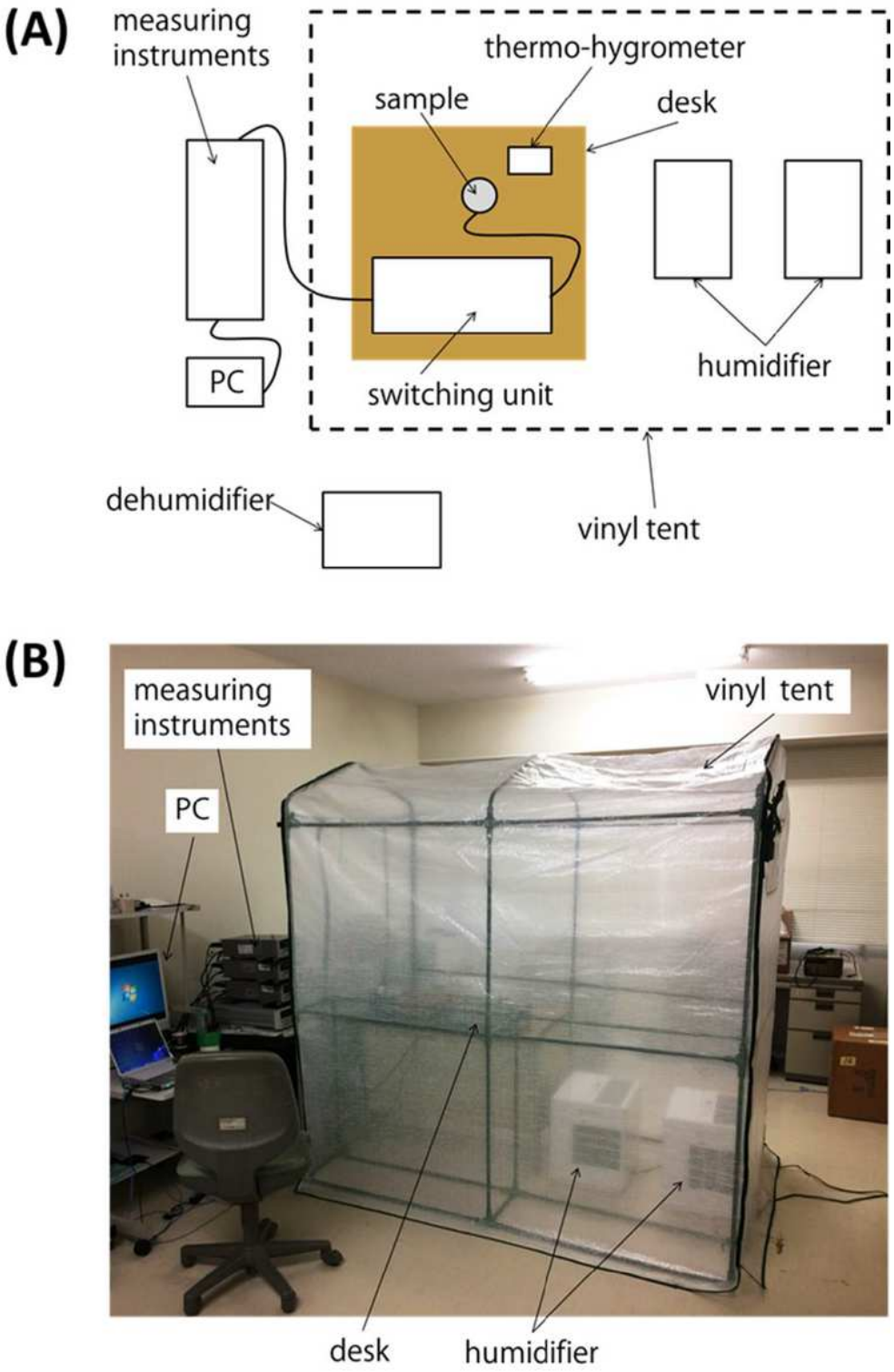

Figure 3

(A) Layout of measurement instrumentation and (B) photograph of the measurement system in the laboratory. Humidity was controlled using a dehumidifier and a humidifier. The vinyl tent was used only when making very high humidity conditions, otherwise each condition was maintained throughout the laboratory. A thermo-hygrometer placed near the sample recorded temperature and humidity. The granite sample, thermo-hygrometer, and switching unit were placed on the same desk. All repeated measurements were performed without direct human intervention, because manual terminal switching and instrument operation would cause serious signal noise. The switching unit performed the connection of terminals and electrodes during repeated measurements. The instruments and switching unit were controlled using LabVIEW software on the PC.

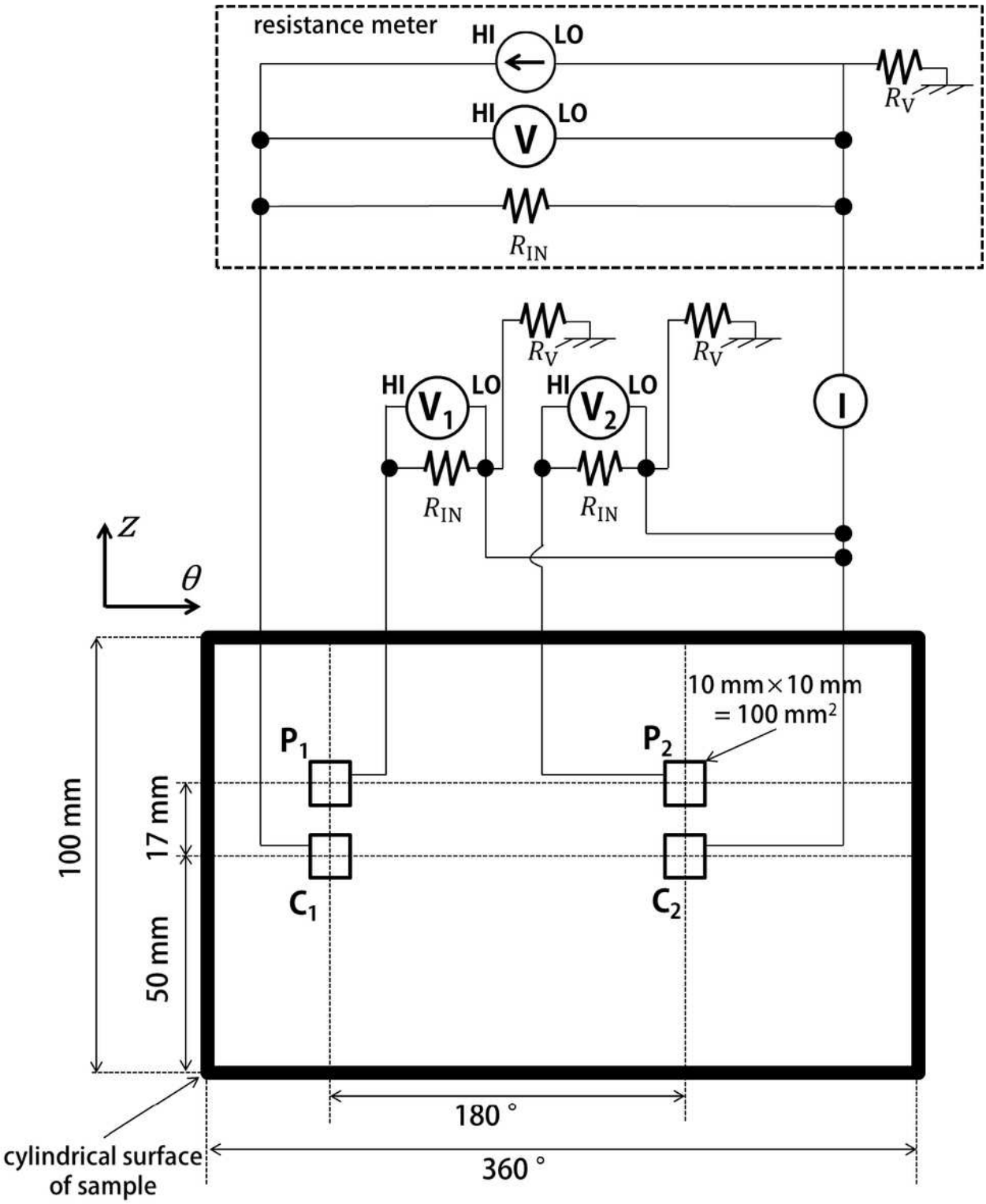

Figure 4

Measurement scheme. z and θ are coordinates defined in Fig. 2(A). The circled arrow is a direct current source, the dotted square is a resistance meter, V1 and V2 are voltmeters, A is an ammeter, RIN is input resistance, RV is insulation resistance between the negative terminal and chassis ground, HI labels positive terminals, LO labels negative terminals, C1 and C2 are current electrodes, and P1 and P2 are potential electrodes. In this study, a resistance meter was used as a direct current source. The resistance

meter injects known direct constant current, measures the voltage caused by injected current, and obtains resistance. An ammeter (Model 3458A, Keysight; Santa Rosa, California, USA) was placed in order to monitor the amount of injected current. Electrometers (Model 6514, Keithley, Cleveland, Ohio, US.) with RIN = 200 TΩ acted as the resistance meter and the voltmeter. Each measuring instrument was connected to the conductive epoxy adhesive used as electrodes shown in Fig. 2 (C).

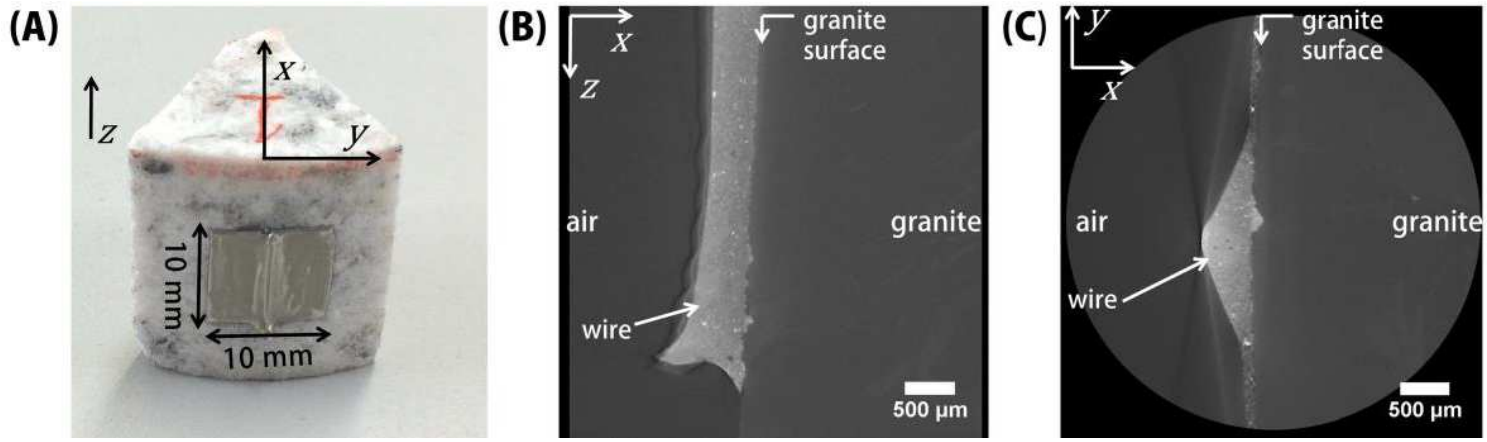

Figure 5

Microstructures of the contact surface observed by micro-focus X-ray computed tomography (CT). (A) Sample photograph showing the 100 mm2 electrode. CT images of the (B) x–z and (C) x–y planes; the pixel size is approximately 4 μm, and the scale bar in each image is 500 μm. Black in the CT images represents areas of X-ray transmission; the white areas are opaque to X-rays. Here, black represents mainly air, dark grey is mainly granite, and light grey is the conductive epoxy adhesive and wires. The images show roughness at the rock sample surface, and the good attachment of the electrodes to this rough surface.

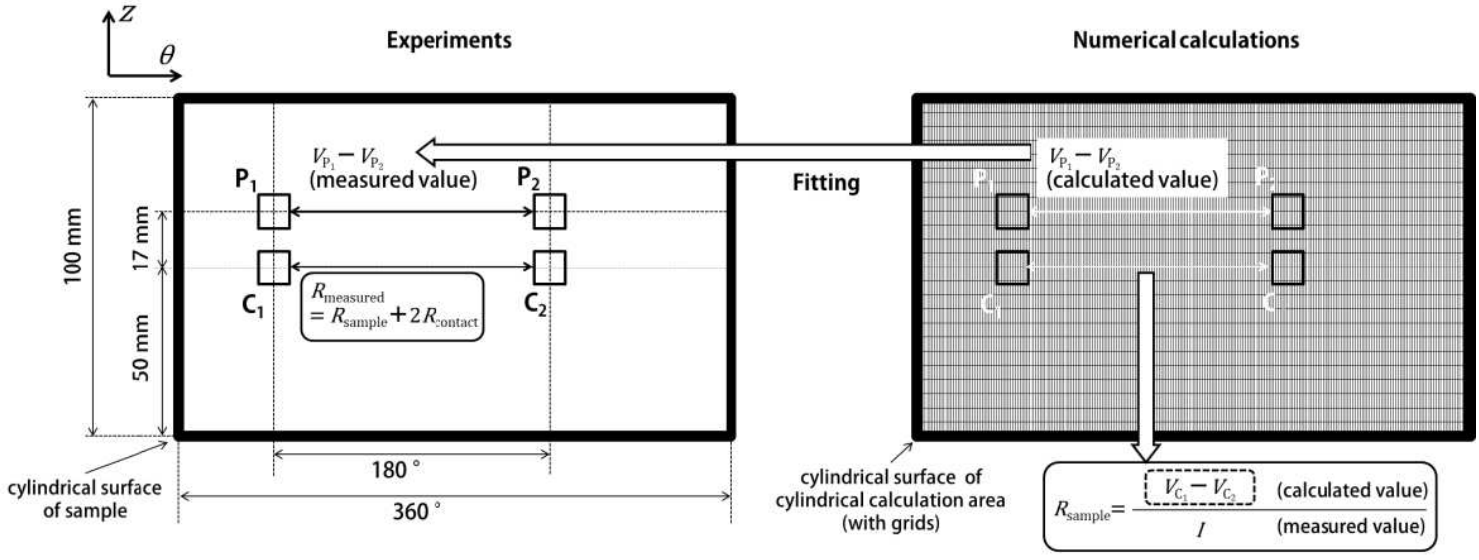

Figure 6

Estimation of resistance between current electrodes. The coordinates z and θ are as defined in Fig. 2(A). C1 and C2 are current electrodes, and P1 and P2 are potential electrodes. and are electrical potential at C1, C2, P1, and P2. Rmeasured, Rsample, and Rcontact are respectively the measured resistance between the current electrodes, the sample resistance between the current electrodes, and the contact resistance at the current electrodes. I is measured current. The left diagram depicts the measurement area (i.e., the sample's side surface), and the right diagram represents the numerical model of the measurement area with its calculation grids. Performing numerical calculations under various sample resistivities searched for a potential distribution that mostly explains the observed . The calculations assumed the sample to have a homogeneous resistivity structure is extracted from the determined potential distribution, and used to obtain Rsample by dividing it by I.

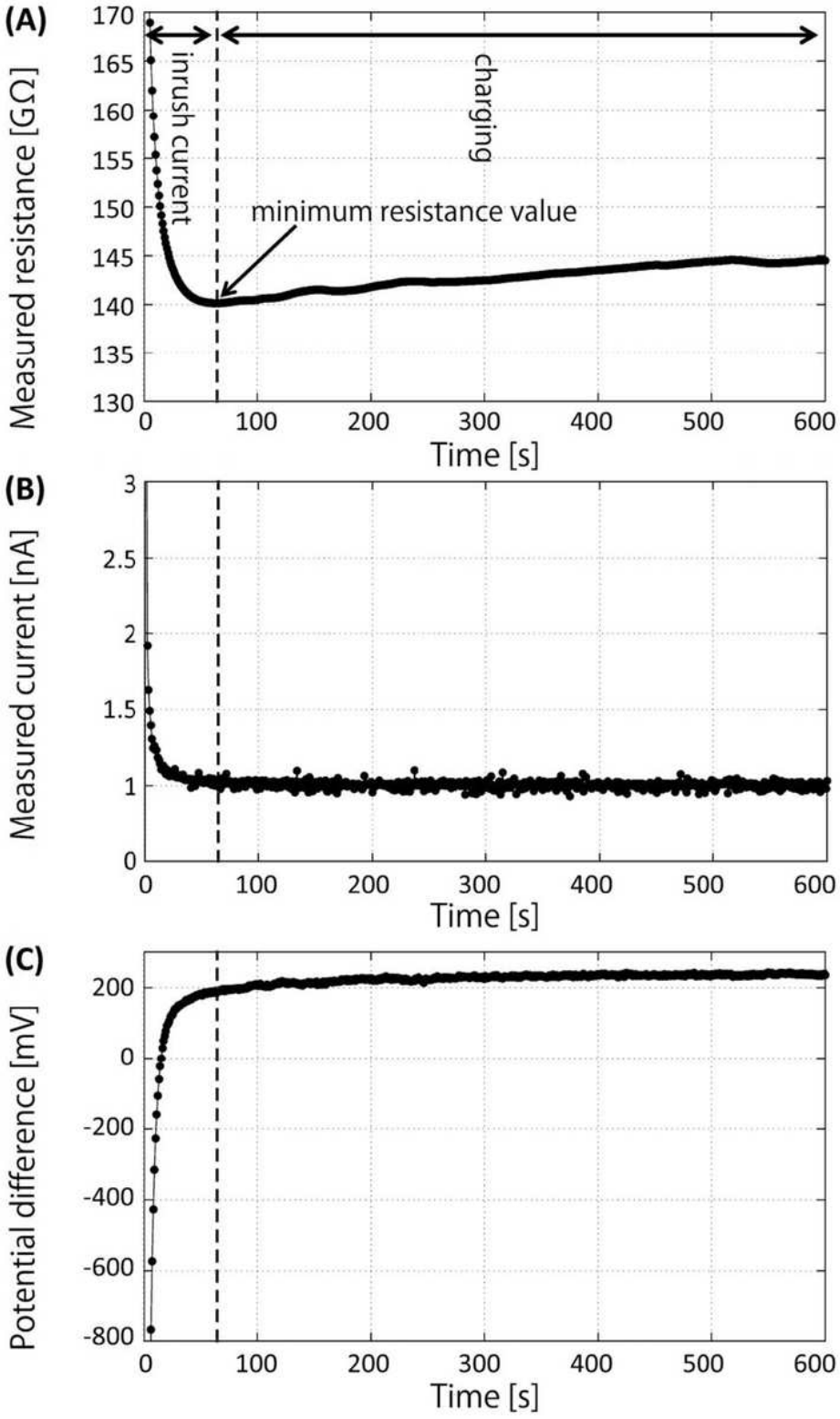

Figure 7

Representative time-series data for resistance, current, and potential difference. The results are those measured for 600 s at 40% relative humidity and 30°C using the measurement layout in Fig. 3. (A) Resistance between C1 and C2 measured by a resistance meter. (B) Current measured by an ammeter. (C) Potential difference between P1 and P2. The injected current took several tens of seconds to stabilise after measurement started. It was initially larger than the specified current used by the resistance meter to

measure resistance in the GΩ range, and was interpreted as inrush current. This inrush current caused the resistance also to take several tens of seconds to stabilise, after which resistance increased. This was interpreted as charging. The minimum in the resistance data for 600 s is therefore considered the most representative value, because the effects of inrush current and charging are likely smallest. Current and potential difference were taken as their values at the time when resistance was lowest, as indicated by the dashed line.

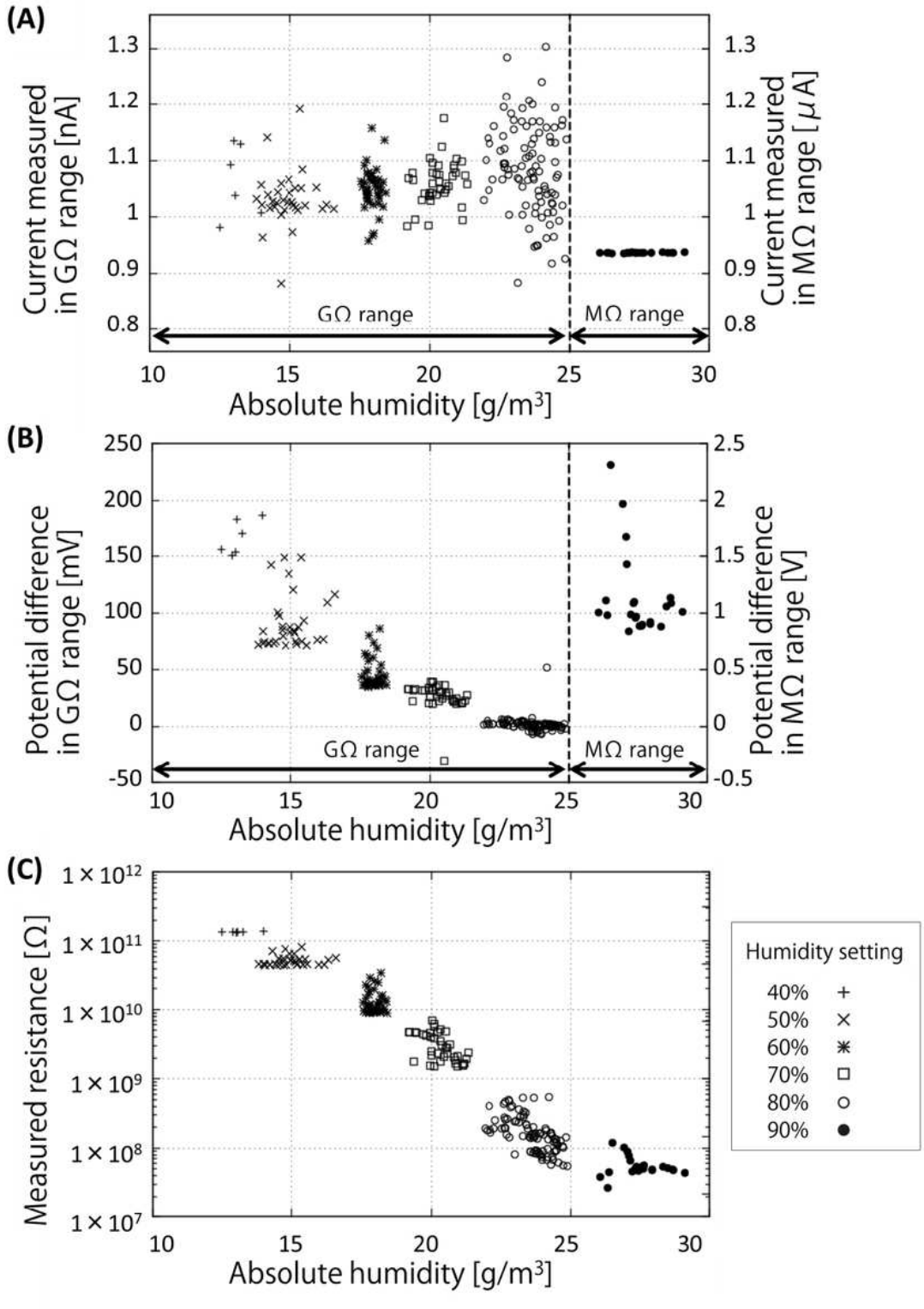

Figure 8

Current, potential difference, and resistance with respect to absolute humidity. (A) Current measured by ammeter and (B) measured potential difference between P1 and P2 as a function of the absolute humidity. (C) Measured resistance between C1 and C2 as a function of the absolute humidity in log scale. Measurements were repeated in six sequences of relative humidity (40%, 50%, 60%, 70%, 80%, and 90%) under constant temperature (30 °C), with the symbols indicating the measurement sequence. Multiple measurements were performed for each sequence to confirm reproducibility. In each sequence, the minimum value observed in 600 s of resistance data was selected and plotted. The plotted current and potential difference are those at the time of minimum resistance. The injected current amount depended on the resistance measurement range (Table 2). The potential difference depended on the current amount difference. Dashed lines indicate the boundary of the measurement range. Each sequence of repeated measurement results shows high repeatability.

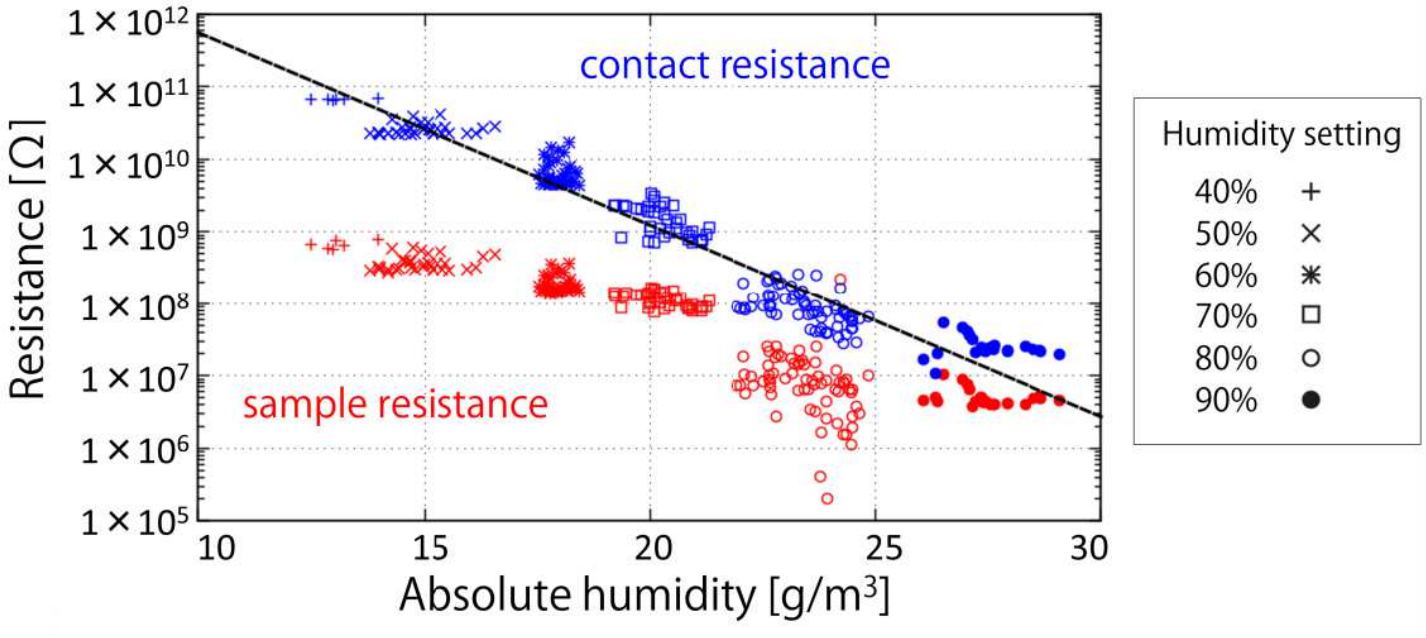

Figure 9

Estimated contact resistance and sample resistance with respect to absolute humidity. Resistances between current electrodes C1 and C2 are plotted as a function of the absolute humidity in log scale. The dashed line represents exponential fitting results, and the symbols indicate the measurement sequence. Sample resistance was estimated numerically from the measured current and potential difference values in Figs. 8(A) and (B). Contact resistance is half of the value obtained by subtracting the estimated sample resistance from the measured resistance value in Fig. 8(C). Both contact resistance and sample resistance decreased exponentially as the absolute humidity increased. Most of the resistance measured by the resistance meter appeared to be contact resistances. The relationship between contact resistance and absolute humidity was mostly represented by an exponential function.

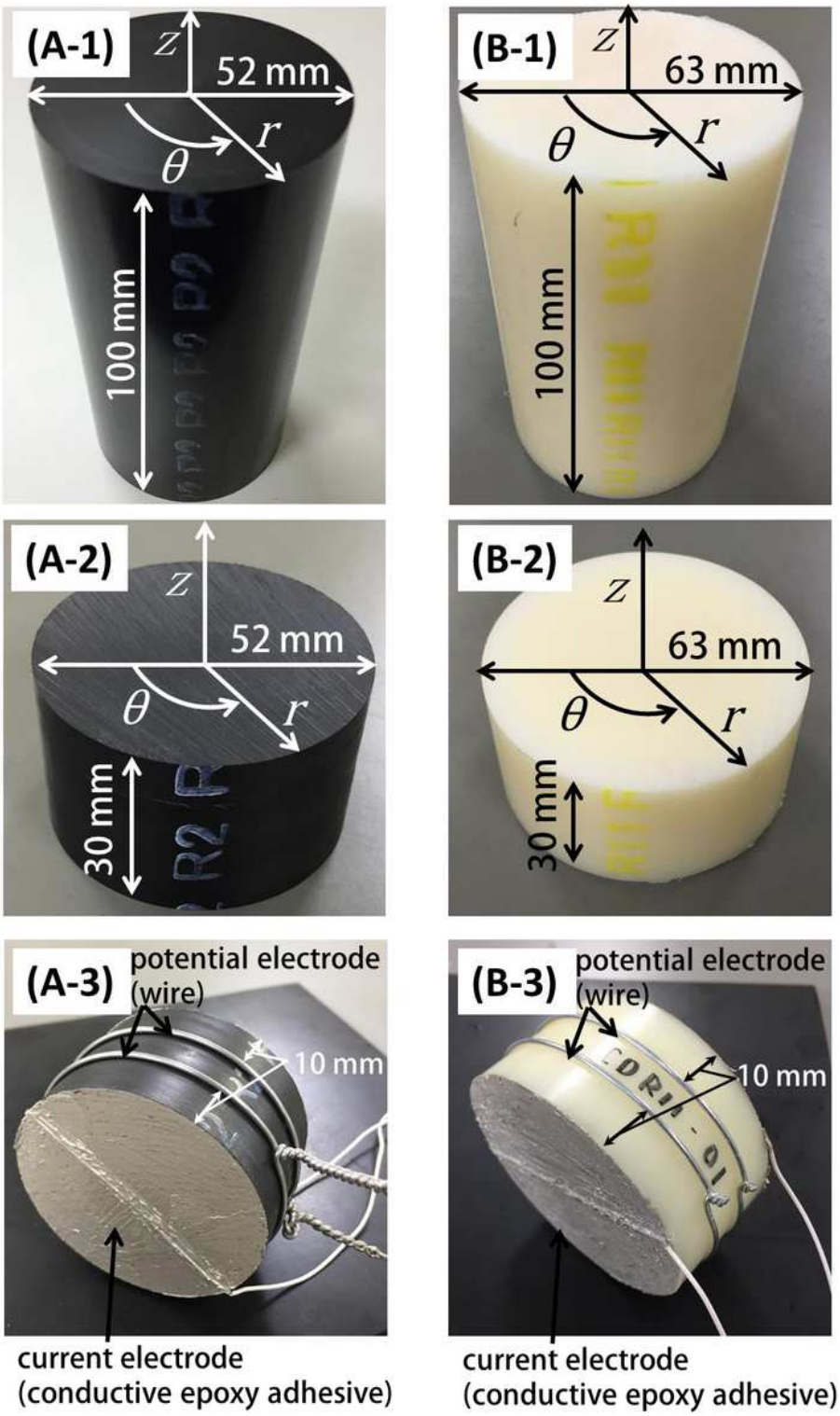

Figure 10

Photographs of set-up for measurement of plastic samples overlaid with the dimensions r, θ, and z defining the coordinate axis. Top row: Cylindrical plastic samples (A-1) MC501CD R2 (Mitsubishi Chemical Advanced Materials, Tokyo, Japan; 52 mm diameter, 100 mm length) and (B-1) MC500AS R11 (Mitsubishi Chemical Advanced Materials, Tokyo, Japan; 63 mm diameter, 100 mm length). Middle row: Thin-disk plastic samples (52 mm diameter, 30 length) of (A-2) MC501CD R2 and (B-2) MC500AS R11.

Bottom row: Arrangement of wire potential electrodes around the thin-disk samples' side surface and conductive epoxy-adhesive current electrodes attached to their ends, (A-3) MC501CD R2 and (B-3) MC500AS R11

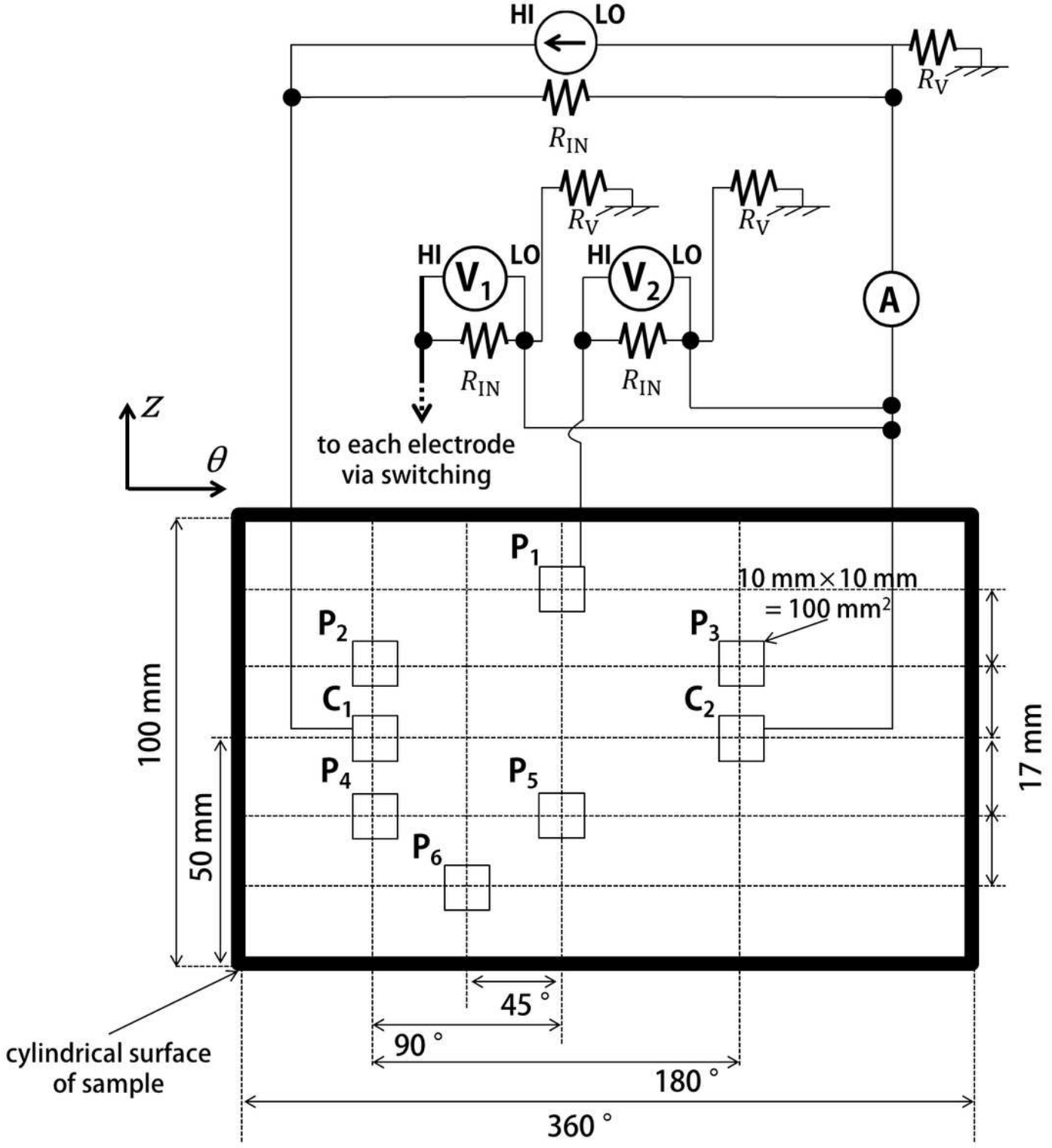

Figure 11

A scheme of measurement for the cylindrical plastic samples. z and θ are coordinates as defined in Fig. 10. The circled arrow is a constant DC source, V1 and V2 are voltmeters, A is an ammeter, RIN is input

resistance, RV is insulation resistance between the negative terminal and chassis ground, HI labels positive terminals, LO labels negative terminals, C1 and C2 are current electrodes, and P1, P2, P3, P4, P5, and P6 are potential electrodes. The DC source (Model 6243, ADC; Saitama, Japan) injected a known constant current. An ammeter (Model 3458A, Keysight; Santa Rosa, California, USA) monitored the injected current. Electrometers (Model 6514, Keithley, Cleveland, Ohio, US.) with RIN = 200 TΩ acted as the voltmeters. Each measuring instrument was connected to the conductive epoxy adhesive used as electrodes shown in Fig. 2 (C).

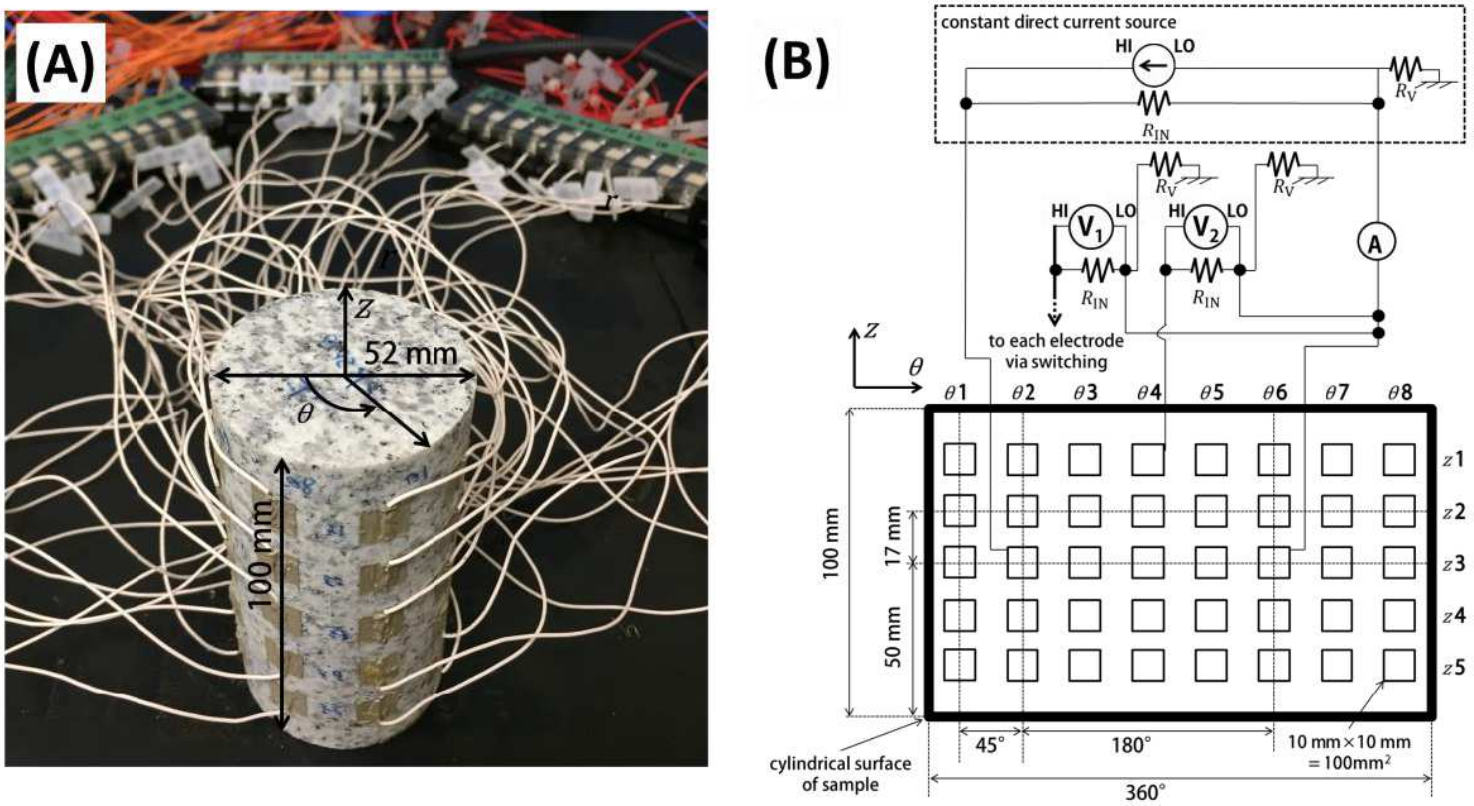

Figure 12

Photograph and schematic diagram of the measurement set-up with an array of electrodes. (A) Cylindrical rock sample (52 mm diameter and 100 mm length) overlaid with the dimensions r, θ, and z defining its coordinate axes. Electrodes were attached to the cylindrical surface, and wires attached to electrodes provided a connection for measuring instruments. (B) Measurement scheme. z and θ are coordinates defined in Fig. 10(A). The dotted square is a constant direct current source, V1 and V2 are voltmeters, A is an ammeter, RIN is input resistance, RV is insulation resistance between the negative terminal and chassis ground, HI labels positive terminals, and LO labels negative terminals. The direct current source (Model 6243, ADC; Saitama, Japan) injected a known constant current. An ammeter (Model 3458A, Keysight; Santa Rosa, California, US.) monitored the amount of injected current. Electrometers (Model 6514, Keithley; Cleveland, Ohio, USA) with RIN = 200 TΩ acted as the voltmeters. Each measuring instrument was connected to the conductive epoxy adhesive used as electrodes as shown in Fig. 2 (C).

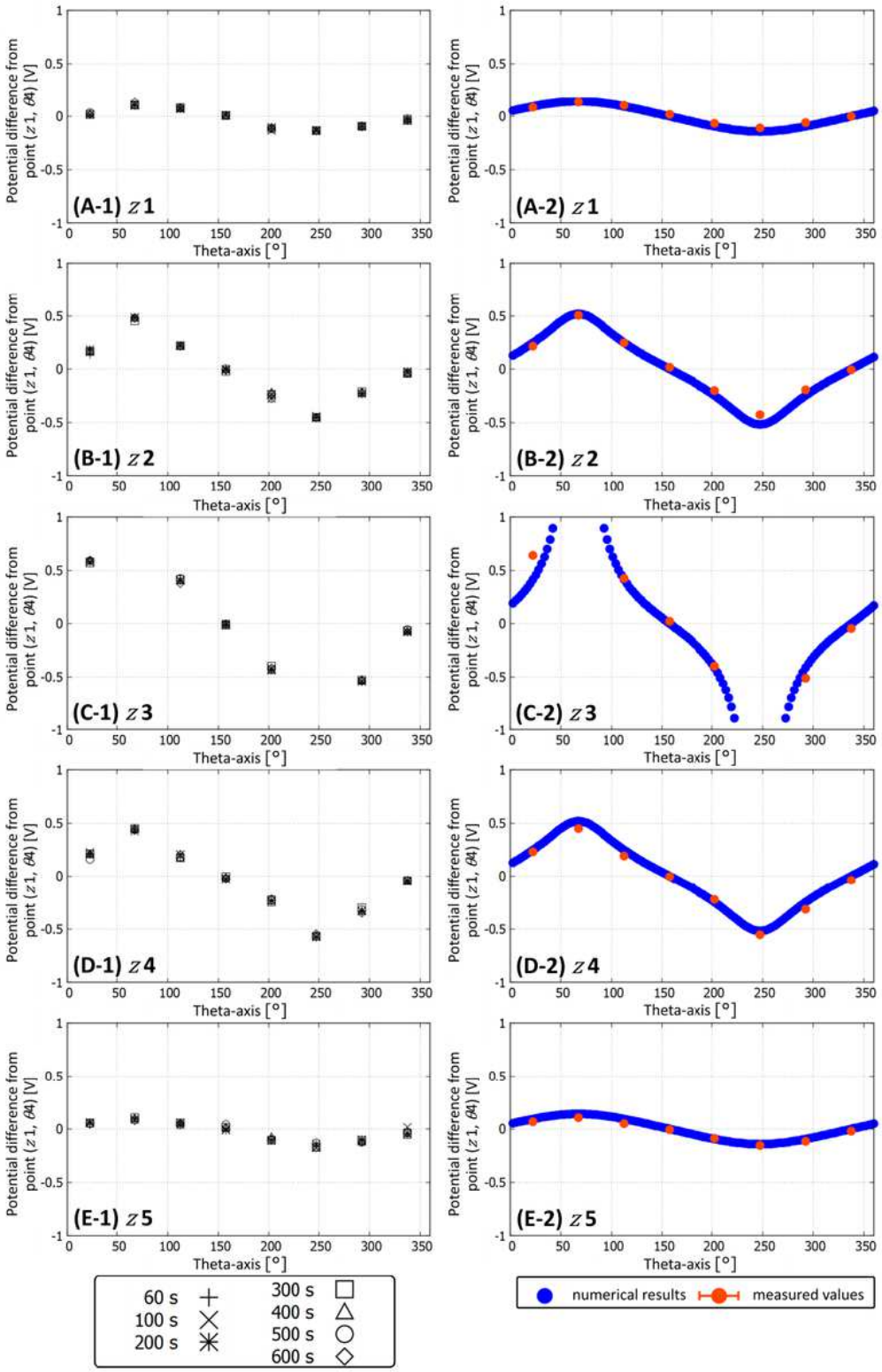

Figure 13

Profiles of electrical potential in the circumferential direction θ at each z from measurements using an electrode array. The coordinates z and θ are defined in Fig. 12. (A) Profile at z1 = 16.7 mm, (B) at z2 = 33.3mm, (C) at z3 = 50 mm, (D) at z4 = 66.7 mm, and (E) at z5 = 83.3 mm. Left panels (A-1 to E-1) show the measured value with elapsed time (60, 100, 200 s, etc.) from the start of the measurement at each potential electrode. The symbols indicate the data acquisition time. The reference point for the measured

potential distribution used for comparison with the numerical results is the midpoint between the current electrodes. Right panels show numerical results of forward modelling (A-2 to E-2). The orange and blue dots respectively indicate the experimental and numerical results. In experimental results, error bars are smaller than the symbols. Each measured value is the potential at each electrode averaged over the last 100 s of measurement. The numerical results were calculated by using the average of all 100 s current intensity data at the corresponding timing of potential observation. The measured values were normalised by the average current for comparison.

Supplementary Files

This is a list of supplementary files associated with this preprint. Click to download.

- TSGraphicalAbstract20210205.png